A Study on Energy Harvesters for Physical Unclonable Functions and Random Number Generation

Erick Aponte

Thesis submitted to the Faculty of the
Virginia Polytechnic Institute and State University
in partial fulfillment of the requirements for the degree of

Master of Science
in
Electrical Engineering

Dong S. Ha, Chair
Qiang Li
Patrick R. Schaumont

June 23, 2017
Blacksburg, Virginia

Keywords: Physical Uncloneable Functions, Random Number Generator, Transducers, Energy Harvesting
Copyright 2017, Erick Aponte

A Study on Energy Harvesters for Physical Unclonable Functions and Random Number Generation

Erick Aponte

(ABSTRACT)

As the broad implementation and use of wireless sensor nodes in Internet of Things (IOT) devices increase over the years, securing personal data becomes a growing issue. Physical unclonable functions (PUFs) and random number generators (RNGs) provide methods to generate security keys for data encryption. Transducers used in the energy harvesting systems of wireless sensor nodes, can generate the PUFs and RNGs. These transducers include piezoelectric devices (piezo), thermoelectric generators (TEG) and solar cells. This research studies the electrical properties of transducers at normal and low operating levels for electrical responses that can be used in PUF generation and random number generation respectively.

The PUF generation discussed in this study analyzes the resonance frequency of 10 piezos, and the open-circuit voltages of 5 TEGs and 5 solar cells. The transducers are tested multiple times over a 10-day period to evaluate PUF reproducibility and reliability characteristics. The random number generation is accomplished by applying a low-level vibration, thermal or light excitation to each respective transducer. The generated electrical signals are amplified and digitally processed and analyzed using the National Institute of Standards and Technology (NIST) Statistical Test Suite.

The experiment results for the PUF generation are promising and indicate that the piezos are the better choice due to their stable frequency output. Each transducer was able to produce random numbers and pass the NIST tests, but the TEGs passed the NIST tests more often than the other transducers. These results offer a preliminary basis for transducers to be used directly in security applications.

A Study on Energy Harvesters for Physical Unclonable Functions and Random Number Generation

Erick Aponte

(GENERAL AUDIENCE ABSTRACT)

As the broad implementation and use of wireless sensor nodes in Internet of Things (IOT) devices increase over the years, securing personal data becomes a growing issue. Physical unclonable functions (PUFs) and random number generators (RNGs) provide methods for securing data. Transducers used in the energy harvesting systems of wireless sensor nodes, can be used to generate the PUFs and RNGs. These transducers convert vibrations, light and heat into electricity. This research studies the electrical properties of transducers at normal and low operating levels for responses that can be used in PUF generation and random number generation respectively.

The PUF generation discussed in this study analyzes the different electrical properties of each transducer. The transducers are tested multiple times over a 10-day period to gather an adequate amount of data. Producing the same output every single time is imperative for PUFs. The random number generation is accomplished by applying a low input vibration, heat or light to each respective transducer. The generated electrical signals are amplified and digitally processed to be analyzed using software.

The experiment results for the PUF generation are promising and indicate that the transducers that convert vibrations to electrical energy are the better choice due to their consistent output. Each transducer was able to produce random numbers and pass the required tests. These results offer a preliminary basis for transducers to be used directly in security applications.

Acknowledgments

I would like to thank my advisor, Dr. Dong S. Ha, for his guidance and support over the last two years while I conducted this research. I would also like to thank Dr. Patrick Schaumont and Dr. Qiang Li for being members of my committee and answering any questions that I had along the way.

I would like to thank the Electrical Engineering Department at Virginia Tech for funding my graduate research studies through teaching assistantships. I would also like to thank Dominion Virginia Power for also granting me the Dominion Virginia Power Research Fellowship.

I would like to thank everyone in the MICS lab: Ji Hoon Hyun, Yudong Xu, Alante Dancy, Nate Turner, Ben Conlon, Joseph Chong, Daniel Herrera, Brannon Kerrigan, Jebreel Salem, Yu Lin, Nan Chen, and Liao Wu. I enjoyed working with you all and going on our semesterly hikes.

Special thanks to everyone at Virginia Tech that made my experience here an amazing one: Dr. Jack Lesko, Dr. Catherine Amelink, Chris O'Lone, Mudit Khanna, Owen Jong, Corey Rhodes, Amy Romero, Joseph Kozak, Victor Turriate, Alex Chu and everyone in the New Horizons Scholars group.

Finally, I am forever grateful to my mom, Ana Tapia, my brother, Kelvin Tejada, my girlfriend, Lisbeth Acosta, and my family from all around the world, including Nagua, Dominican Republic for all of your unconditional support and love.

Contents

List of Figures

List of Tables

Chapter 1

Introduction

1.1 Motivation

Wireless sensor nodes have existed for decades to compose wireless sensor networks for a variety of applications ranging from air pollution monitoring to military warfare [1]. Many of today's modern electronics include these wireless sensor nodes and are interconnected by the Internet of Things (IoT). Experts estimate that by 2020, there will be over 20 billion IoT devices collecting and exchanging data [2]. Nonetheless, these wireless sensor nodes pose challenges due to various resource constraints regarding energy, computational power and memory allocation [3, 4, 5, 6]. Modern wireless sensor nodes have addressed energy constraints by adopting energy harvesting systems as a power source in lieu of standalone batteries [7, 8]. With the implementation of a longer-lasting power source, wireless sensor nodes can be powered for an extended period of time and collect more data.

The data collected by the wireless sensor nodes are often regarded as confidential or sensitive and must remain secure when communicating with other sensor nodes within the network [9]. This is especially true for wireless sensor nodes scattered in human-accessible areas or hostile environments where they are more prone to physical attacks [10, 5]. Security techniques used in traditional networks cannot be applied directly because of the architecture and nature of the wireless sensor node [9].

One of the first requirements when setting up a wireless sensor network, is to establish cryptographic keys for each sensor node. Typically these keys are generated from computational algorithms or by using unique features of the wireless sensor network itself [11, 9]. This research focuses on discovering potential sources for key generation from the energy harvesting component of wireless sensor nodes, specifically transducers, to work in conjunction with existing methods.

1.2 Energy Harvesting

A typical wireless sensor node is comprised of a power source, microcontroller, transceiver, external memory and one or more sensors as shown in Figure 1.1.

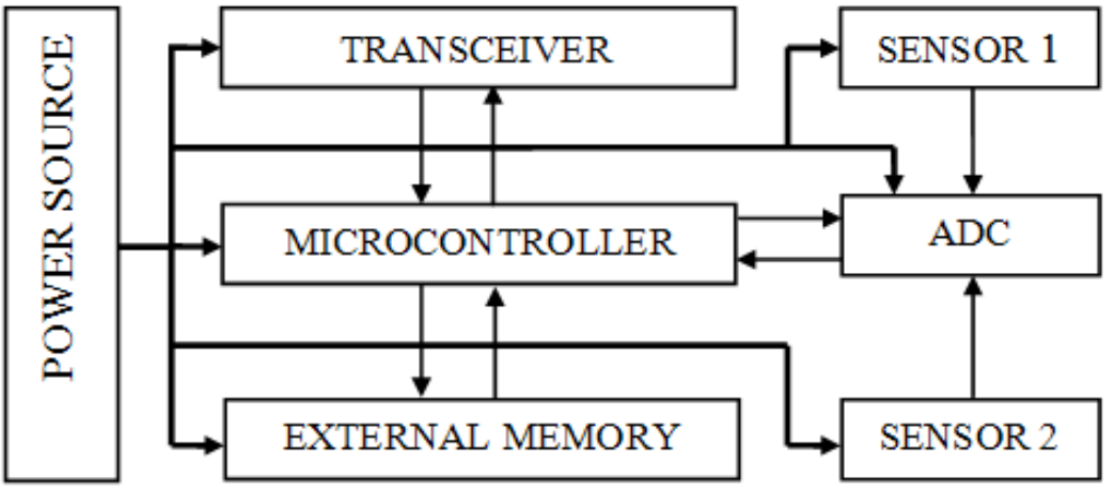

Figure 1.1: Block Diagram of a Wireless Sensor Node [12].

This paper focuses on the power source portion of the sensor node architecture, which typically is an energy harvesting system. As shown in Figure 1.2, a standard energy harvesting system includes the ambient energy source, the power management system and the load. The idea behind this research is to use the transducer more directly with the sensor node.

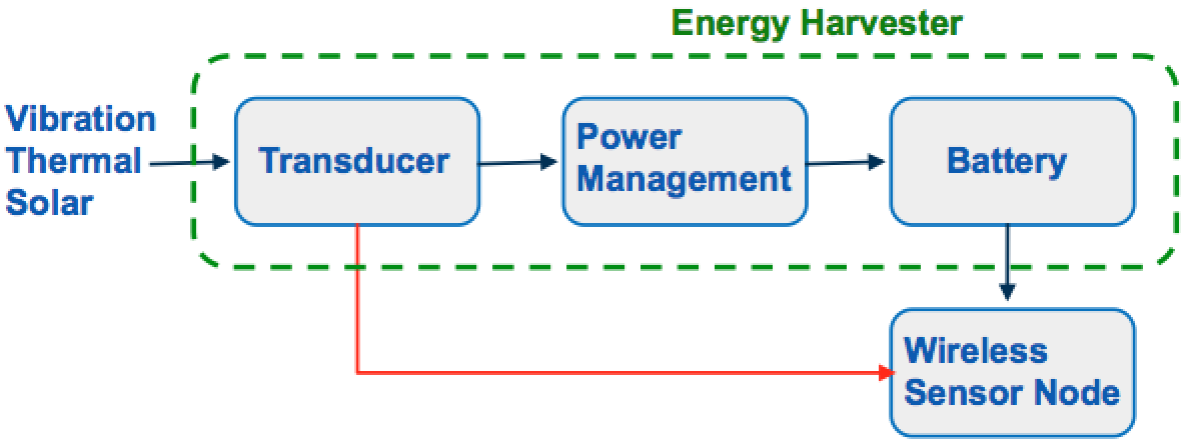

Figure 1.2: Basic Block Diagram of an Energy Harvesting System.

The ambient energy sources discussed in this paper are vibration, thermal and solar. The corresponding transducers for these sources are piezoelectric devices, thermoelectric generators and solar cells respectively. The piezoelectric device converts mechanical vibrations into an electrical output. Thermoelectric generators generate a voltage potential proportional to the temperature gradient across them. The solar cells convert light into electricity using the photoelectric effect.

1.3 Existing Methods for PUF and Random Number Generation

A PUF is the hardware version of a one-way function embodied in a physical structure that exploits the physical manufacturing variations of said structure to map different outputs to their respective inputs [13, 14]. There a many different methods of generating PUFs, but this section will focus on three specific types of PUFs because of their popularity in the field, and close association to the PUFs discussed in Chapter 3.

The ring oscillator PUF is a device composed of an odd number of NOT gates that produces an oscillatory output between two voltage levels [15]. Each NOT gate contributes a delay to the output signal where the output frequency depends on the total delay line of the ring oscillator. Due to manufacturing variations when producing the NOT gates, the delay for each NOT gate will essentially be random, and the output frequency of the ring oscillator will also be random, thus creating the PUF.

An optical PUF, requires more of an intricate setup. It shines a laser beam on a pane of transparent material doped with light-scattering particles that produce a unique speckle pattern when excited by the laser beam [15]. The speckle pattern changes as the laser beam orientation onto the transparent material changes location and angle. Since the doping levels between two similar transparent materials will not be the same, the laser beam focused on the exact same spot and angle on both materials, will not produce the same speckle pattern output.

The LC PUF consists of two metal plates and a metal coil to form a passive LC circuit. When performing a frequency sweep on the LC circuit, the resonance frequencies will differ between similar looking systems because of the dependence on the capacitance and inductance of the metal materials [15]. Because of the manufacturing variations, it is difficult for the capacitive and inductive materials to have the exact same values.

There are pseudo random number generators that use computer algorithms and hardware random number generators that utilize noise sources [16]. For the essence of this section and paper, only hardware random generators are discussed and are considered to be non-true random number generators.

Most hardware random number generators utilize noise sources that are known to have a

Gaussian distribution which allows for random outputs to be produced [16]. The BitBabbler uses a combination of shot noise, Johnson noise, flicker noise and avalanche breakdown noise from passive and analog components [17]. The OneRNG random number generator collects entropy from an avalanche diode circuit with an additional whitening block [18]. The QNG Model PQ4000KS harnesses entropy from shot noise due to sub-threshold leakage and gate tunneling leakage in MOS transistors [19].

1.4 Contributions of Proposed Research

This research analyzes transducers, typically used in energy harvesting systems, to support the hypothesis that they may also be used for secure key generation in wireless sensor nodes through the utilization of PUFs and random number generators. The electrical characteristics of the transducers are studied to determine which of those properties produce unique outputs that may be used in PUFs. The intrinsic features of the transducers are also observed for potential noise generating sources that may be utilized in random number generation.

- The series resonance and parallel resonance frequencies of the piezoelectric devices are measured and analyzed for PUF characteristics. The open circuit voltages of the thermoelectric generators and solar cells are measured for their own unique PUFs. Each transducer is tested under normal operation conditions.
- The transducer's electrical output is measured when a corresponding low-level impulse (e.g. vibration, thermal gradient and light intensity) is applied to the input of the transducers. The output is then amplified and recorded for further statistical analysis via the NIST Statistical Test Suite. The analyzed data is a combination of intrinsic noise and measured fluctuations of the applied low-level impulse.

1.5 Organization of Thesis

The organization of this thesis is as follows. Chapter 2 provides background information on PUFs and their qualities and characteristics used to evaluate the transducer-based PUFs. The potential noise sources within the transducers are also discussed, along with the NIST Statistical Test Suite used to evaluate the randomly generated noise data. Chapter 3 details the proposed methods and basis regarding the testing for PUFs and random number generation unique to each type of transducer. Chapters 4 and 5 describe the experiment setups and reports the measurement results, concluding with a comparison of the results among the three different transducers. Lastly, Chapter 6 concludes the paper by reviewing key contributions and recommending transducers for either PUF or random number generation applications.

Future work and directions for improvement of evaluations and testing are also discussed in Chapter 6.

Chapter 2

Preliminaries

This chapter provides background information on PUFs and random number generator sources, along with the analytical processing of the data. Section 2.1 describes the characterizing features of PUFs and its categorical classification. Section 2.2 focuses on noise sources generated from piezoelectric materials and semiconductor materials found in thermoelectric generators and solar cells. Lastly, Section 2.3 provides background on hypothesis testing and the NIST Statistical Test Suite, describing the functions of each test.

2.1 PUF Characteristics

This section provides an introduction into PUF characteristics based on challenge-response behavior and the classification of PUFs based on the number of challenge-response pairs.

2.1.1 Reproducibility and Reliability

A PUF employs a challenge-response pair mechanism, where the challenge is traditionally understood to be the input, and the response is the output of the physical unclonable function as shown in Figure 2.1.

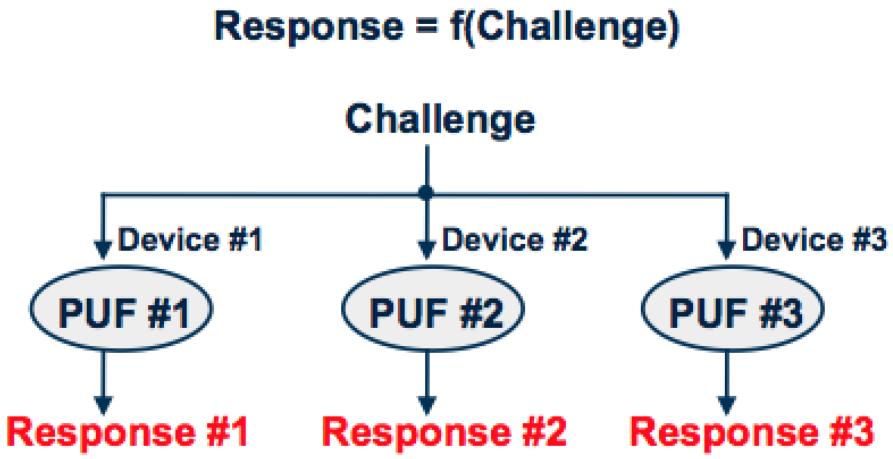

Figure 2.1: Basic Block Diagram of a Physical Unclonable Function.

There are many characterizing features for PUFs that analyze the challenge-response mechanism, but for the scope of this paper the main focus is on reproducibility and temperature reliability. Reproducibility is defined as the ability to evaluate responses from the same given challenge and verify that they are the same or highly similar. Figure 2.2 shows a diagram of this concept.

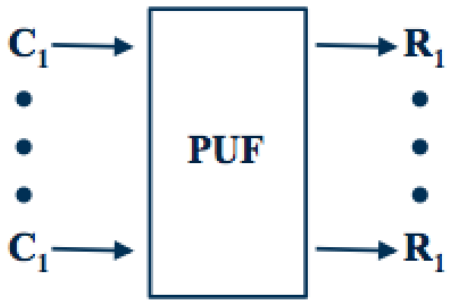

Figure 2.2: Reproducibility of Physical Unclonable Function Responses.

Variability in the responses can often be compensated for by using computer processing methods, but is costly and is only feasible if the variability is relatively low. Noise and environmental factors are typical reasons behind these fluctuations. This leads to the other characteristic of a PUF, temperature reliability. Temperature reliability is defined as the ability to produce the same or closely similar response for a given challenge under various temperature conditions. Since PUFs take advantage of physical manufacturing variations, those same variations can change the underlying properties of the PUF at lower or higher temperature conditions.

2.1.2 Weak PUFs vs. Strong PUFs

PUFs are categorized into two groups, Strong PUFs and Weak PUFs, based on three assumptions [20]. These assumptions state that responses to different challenges are independent of each other, predicting responses that have not been previously observed is difficult and tampering with a PUF instance significantly alters the challenge-response behavior. In practice, if a PUF can generate an exponentially large number of challenge-response pairs, it is considered a strong PUF because it will increase the difficulty for an adversary to model the PUF [21]. Strong PUFs are typically used for authentication applications. With a small number of challenge-response pairs, an adversary can model the PUF rather quickly, and therefore this is considered a weak PUF. Weak PUFs are typically used for key generation purposes.

2.2 Noise Sources

This section details the various noise sources found in the tested piezoelectric devices, thermoelectric generators and solar cells. These noise sources are found in the composition of the transducers through their ceramic, polymer and semiconductor structures.

2.2.1 Piezoelectric Materials

Thermal noise and polarization noise are the major noise sources in piezoelectric ceramics, contributing to voltage or current fluctuations [22]. The tested PZT and PVDF transducers also contain pyroelectric properties that contribute to voltage fluctuations on the output. Figure 2.3 shows a cross section of a piezoelectric transducer and the ceramic foil component of its structure.

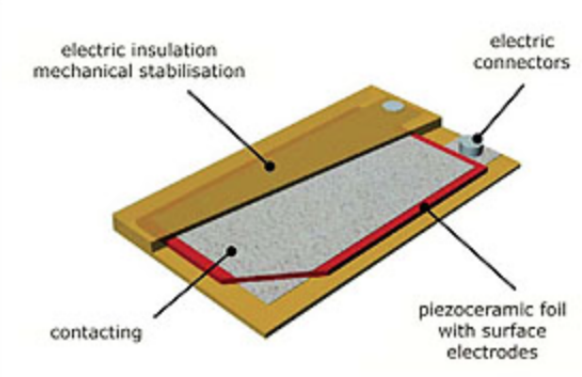

Figure 2.3: Cross Section of a Ceramic Piezoelectric Device [23].

Thermal noise occurs when electrons and other charged carriers in a conductor are thermally agitated and create a temperature dependent random motion of carriers [22, 24].

Polarization noise in piezoelectric ceramics is attributed to the vibrating electrical dipoles. The dipole's vibration is caused by interactions with phonons and creates electrical charges on the electrodes, which is seen as a voltage fluctuation[22].

The pyroelectric properties of the transducers allow for a voltage to be produced when the transducer exhibits a temperature change over time. Temperature fluctuations over time, will generate voltage fluctuations on the output [25].

2.2.2 Semiconductor Materials

As seen in the cross sections of Figure 2.4, a typical thermoelectric generator and solar cell are composed of pn thermocouples and junctions. These pn thermocouples and junctions house the majority of the noise sources found in each transducer. The several noise sources include thermal noise as described above, shot noise and generation-recombination noise [24].

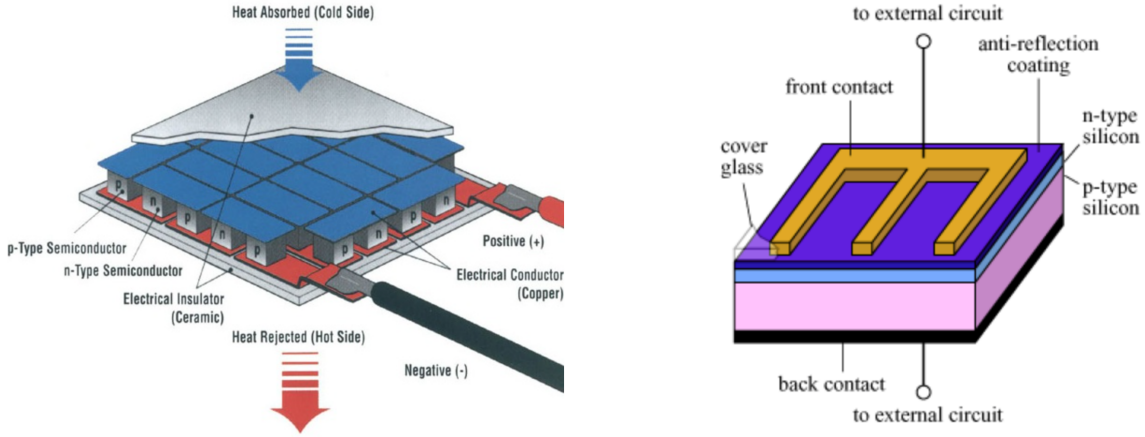

(a) Thermoelectric Generator [26].

(b) Solar Cell [27].

Figure 2.4: Cross Sections of a Thermoelectric Generator and Solar Cell.

Shot noise is produced by carrier injection through the pn junction when a carrier has enough thermal energy to overcome the potential barrier within a forward-bias junction. Mobility increases with temperature and the number of carriers that can overcome this barrier is random [24].

Generation-recombination noise occurs when carrier concentration fluctuates and randomly transition between different states along the energy band [28].

2.3 Statistical Analysis

This section describes the process of hypothesis testing and provides a detailed description of the 15 different tests from the NIST Statistical Test Suite.

2.3.1 Hypothesis Testing

A hypothesis test is a form of a statistical test formulated to test a null hypothesis H_0. The null hypothesis in this paper states that the data sequence under test is random and the alternative hypothesis, H_A, states that the data sequence is not random. Typically the conclusion of the hypothesis states that the one either rejects the null hypothesis, or fails to reject the null hypothesis based on the gathered tested data.

The generated data sequence from the random number generator is tested via the 15 different hypothesis tests in the NIST Statistical Test Suite. A set of p-values is generated from the tests along with a specific test statistic that is used to determine the random quality of the the tested data sequence. The test statistic is used to calculate p-values of a data sequence for a certain distribution [29]. P-values evaluate how well the tested data sequence supports the null hypothesis, H_0, that the data sequence is random. A significance level, α, is determined and typically ranges from 0.01 to 0.05 depending on the test and application. If the p-value is larger than α, it is determined that one fails to reject the null hypothesis. A p-value smaller than α, concludes that the null hypothesis is rejected.

2.3.2 NIST Statistical Test Suite

The NIST Test Suite consists of 15 tests that were developed to test the randomness of generated binary sequences from hardware random number generators and other types of random number generators. The 15 tests are:

- **Test #1** Frequency (Monobit) Test
- **Test #2** Frequency Test within a Block
- **Test #3** Runs Test
- **Test #4** Longest-Run-of-Ones in a Block Test
- **Test #5** Binary Matrix Rank Test
- **Test #6** Discrete Fourier Transform Test
- **Test #7** Non-overlapping Template Matching Test
- **Test #8** Overlapping Template Matching Test
- **Test #9** Maurer's "Universal Statistical" Test
- **Test #10** Linear Complexity Test
- **Test #11** Serial Test
- **Test #12** Approximate Entropy Test

- **Test #13** Cumulative Sums Test
- **Test #14** Random Excursions Test
- **Test #15** Random Excursions Variant Test

The Frequency (Monobit) Test focuses on the proportion of zeroes and ones for the entire sequence. The purpose of this test is to determine whether the number of ones and zeros in a sequence are approximately the same as would be expected for a truly random sequence. The test assesses the closeness of the fraction of ones to 12, that is, the number of ones and zeroes in a sequence should be about the same. All subsequent tests depend on the passing of this test [29].

The Frequency Test within a Block focuses on the proportion of ones within M-bit blocks. The purpose of this test is to determine whether the frequency of ones in an M-bit block is approximately M/2, as would be expected under an assumption of randomness [29].

The Runs Test focuses on the total number of runs in the sequence, where a run is an uninterrupted sequence of identical bits. A run of length k consists of exactly k identical bits and is bounded before and after with a bit of the opposite value. The purpose of the runs test is to determine whether the number of runs of ones and zeros of various lengths is as expected for a random sequence. In particular, this test determines whether the oscillation between such zeros and ones is too fast or too slow [29].

The Test for the Longest Run of Ones in a Block focuses on the longest run of ones within M-bit blocks. The purpose of this test is to determine whether the length of the longest run of ones within the tested sequence is consistent with the length of the longest run of ones that would be expected in a random sequence [29].

The Binary Matrix Rank Test focuses on the rank of disjoint sub-matrices of the entire sequence. The purpose of this test is to check for linear dependence among fixed length substrings of the original sequence [29].

The Discrete Fourier Transform (Spectral) Test focuses on the peak heights in the Discrete Fourier Transform of the sequence. The purpose of this test is to detect periodic features (i.e., repetitive patterns that are near each other) in the tested sequence that would indicate a deviation from the assumption of randomness. The intention is to detect whether the number of peaks exceeding the 95% threshold is significantly different than 5% [29].

The Non-overlapping Template Matching Test focuses on the number of occurrences of pre-specified target strings. The purpose of this test is to detect generators that produce too many occurrences of a given non-periodic (aperiodic) pattern. For this test and for the Overlapping Template Matching test of Section 2.8, an m-bit window is used to search for a specific m-bit pattern. If the pattern is not found, the window slides one bit position. If the pattern is found, the window is reset to the bit after the found pattern, and the search resumes [29].

The Overlapping Template Matching Test focuses on the number of occurrences of

pre-specified target strings [29].

The Maurers Universal Statistical Test focuses on the number of bits between matching patterns (a measure that is related to the length of a compressed sequence). The purpose of the test is to detect whether or not the sequence can be significantly compressed without loss of information [29].

The Linear Complexity Test focuses on the length of a linear feedback shift register (LFSR). The purpose of this test is to determine whether or not the sequence is complex enough to be considered random. Random sequences are characterized by longer LFSRs. An LFSR that is too short implies non-randomness [29].

The Serial Test focuses on the frequency of all possible overlapping m-bit patterns across the entire sequence. The purpose of this test is to determine whether the number of occurrences of the 2m m-bit overlapping patterns is approximately the same as would be expected for a random sequence. Random sequences have uniformity; that is, every m-bit pattern has the same chance of appearing as every other m-bit pattern [29].

The Approximate Entropy Test compares the frequency of overlapping blocks of two consecutive and adjacent lengths (m and m+1) against the expected result for a random sequence [29].

The Cumulative Sums (Cusum) Test focuses on the maximal excursion (from zero) of the random walk defined by the cumulative sum of adjusted (-1, +1) digits in the sequence. The purpose of the test is to determine whether the cumulative sum of the partial sequences occurring in the tested sequence is too large or too small relative to the expected behavior of that cumulative sum for random sequences [29].

The Random Excursions Test focuses on the number of cycles having exactly K visits in a cumulative sum random walk. The cumulative sum random walk is derived from partial sums after the (0,1) sequence is transferred to the appropriate (-1, +1) sequence [29].

The Random Excursions Variant Test focuses on the total number of times that a particular state is visited (i.e., occurs) in a cumulative sum random walk. The purpose of this test is to detect deviations from the expected number of visits to various states in the random walk [29].

Chapter 3

Proposed Methods for PUF and Random Number Generation

This chapter describes the proposed methods for PUF and random number generation of each transducer. The PUFs must originate from transducer parameters that would be significantly altered due to physical manufacturing variations, creating different measurement readings of the same characteristic for each transducer. Section 3.1 analyzes electrical equations of each transducer related to its corresponding PUF. Section 3.2 discusses how noise is generated from each transducer.

3.1 Physical Uncloneable Function

This section describes the corresponding equations for each transducer that contains variable parameters dependent on manufacturing variations.

3.1.1 Piezo PUF

The piezoelectric devices used in this research are the ceramic based PZT and polymer based PVDF in the shape of a rectangular plate. These transducers generate a voltage potential directly proportional to an applied mechanical strain, force or pressure. Piezoelectric transducers mounted in a cantilever position are free to oscillate after a mechanical force is applied. The resulting electrical output signal will then oscillate at the transducer's resonance frequency. Impedance measurement curves for each transducer will show an impedance minimum at series resonance and an impedance maximum at parallel resonance, unique to each transducer. A simplified resonator circuit as seen in Figure 3.1 can be used to model the transducer around the operating resonance frequency, where L is the mechanically equivalent

inductance proportional to mass, C_1 is the mechanically equivalent capacitance inversely proportional to stiffness, C_0 is the electrical capacitance between the two electrodes of the transducer and R is representative of the losses.

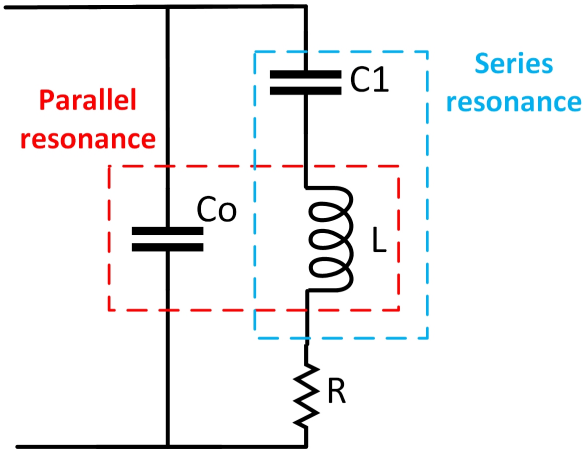

Figure 3.1: Butterworth-van-Dyke (BvD) Equivalent Circuit.

The impedance response of each transducer is measured using an impedance analyzer. The resonance and parallel resonance frequencies are then extracted from the impedance response curves. Equations 3.1 and 3.2 demonstrate the dependence of the series resonance and parallel resonance frequencies on the corresponding inductive and capacitive components.

$$\text{Series Resonance} = \frac{1}{2\pi\sqrt{LC_1}} \tag{3.1}$$

$$\text{Parallel Resonance} = \frac{1}{2\pi\sqrt{LC_0}} \tag{3.2}$$

Although the piezoelectric transducers are designed to be the same shape and volume, because of the many process variations during the manufacturing of the transducers, The frequencies will differ between each transducer due to the response's dependence on physical parameters that are difficult replicate for each transducer.

3.1.2 TEG PUF

Thermoelectric generators are composed of thermopiles or also named thermocouples, electrically interconnected in series and thermally connected in parallel. Each thermopile or thermocouple is composed of n-type and p-type semiconductor material pair connected in series. The n-type semiconductor material is doped such that the charge carriers and Seebeck

coefficient is negative. The p-type semiconductor material is doped such that the charge carriers and Seebeck coefficient is positive. Since each thermopile generates a low output voltage, typical thermoelectric generators use a large number of thermopiles to produce a larger output voltage. Figure 3.2 shows the equivalent circuit of a TEG and where the open-circuit voltage is measured from.

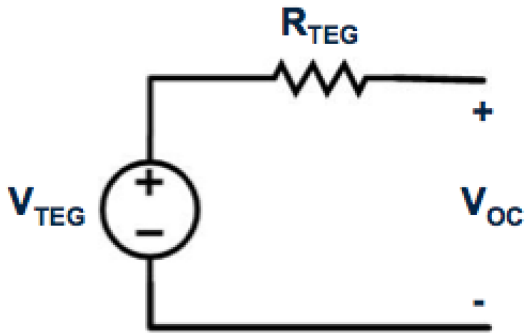

Figure 3.2: Thermoelectric Generator Equivalent Circuit.

The generated power in the thermoelectric generators is attributed to the Seebeck Effect. The Seebeck Effect produces an electric current when dissimilar electrical conductors or semiconductors are exposed to a temperature gradient. Equation 3.3 shows the relationship between the generated output open-circuit voltage V_{OC}, and the Seebeck Coefficient S, the number of thermocouples N and the temperature difference ΔT [30].

$$V_{OC} = S \cdot N \cdot \Delta T \tag{3.3}$$

When one side of the thermoelectric generator is heated, the heated electrons move towards the cooler side of the thermoelectric generator, producing an electrical current when an external load is applied to the output of the thermoelectric generator. The Seebeck Coefficient is dependent on the doping levels of the n-type and p-type semiconductor materials used to create the thermocouples. Therefore, because of the different doping levels caused by process variations during manufacturing, the Seebeck coefficient changes amongst the thermoelectric generators and each thermoelectric generators produces a different open-circuit voltage V_{OC}, for the same ΔT.

3.1.3 Solar Cell PUF

Solar cells are composed of pn junctions typically made of some form of silicon or other semiconductor materials that convert light into electricity. Light particles, known as photons, from light sources collide with the surface of the cell and penetrates into the pn junction.

Here, the photons transfer their energy to the electrons, giving the electrons enough energy to overcome the barrier and form an electrical current in the solar cell when a load is attached. This is caused by the photoelectric effect. Figure 3.3 shows the equivalent circuit model for a solar cell.

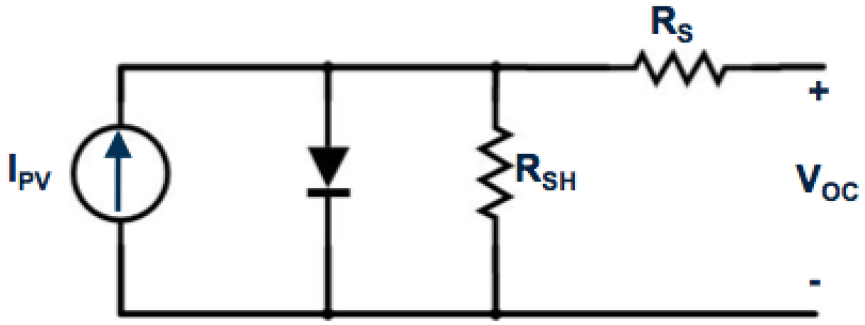

Figure 3.3: Solar Cell Equivalent Circuit.

The photoelectric effect in solar cells allow for a voltage potential to be generated across the solar cell. The generated open-circuit voltage V_{OC} is a function of carrier concentration as seen in Equation 3.4, where $\frac{kT}{q}$ is the thermal voltage, N_A is the doping concentration, Δn is the excess carrier concentration and n_i is the intrinsic carrier concentration [31].

$$V_{OC} = \frac{kT}{q} ln \left[\frac{(N_A + \Delta n)\Delta n}{n_i^2} \right] \tag{3.4}$$

The open-circuit voltage V_{OC} is dependent on the doping concentrations of the semiconductor materials in the pn junctions used to create a solar cell. Therefore, because of the different doping concentrations caused by process variations during manufacturing, the open-circuit voltage V_{OC} changes from one solar cell to another and each solar cell produces a different open-circuit voltage V_{OC}, for the same light intensity.

The solar cells produce an output voltage at different light intensities. The open-circuit voltage of each solar cell is measured over a 30-minute window. This allows enough time for the environment temperature and output voltage to reach steady state levels. Once the temperature has reached steady state, the average value of the open-circuit voltage is measured.

3.2 Random Number Generation

This section discusses the approach to generate a measurable noise signal from each transducer.

3.2.1 Piezo Random Number Generation

The thermal noise and polarization noise sources discussed in Section 2.2.1 contributes to the noise signal output from the piezoelectric transducers. The noise signal from the piezoelectric transducer is generated by first applying a weak low amplitude vibration signal to the transducer. The measured output from the transducer is a relatively weak signal in the microvolts to millivolts range and must be amplified with an external amplifier circuit. The amplified signal is then sampled/recorded with a data acquisition tool for further statistical analysis. Figure 3.4 demonstrates the basic block diagram of the piezo RNG. A shaker is used to produce the low-level excitation and the piezo outputs a noisy signal.

Figure 3.4: Block Diagram of Piezo Random Number Generator.

The analyzed noise signal is a combination of the applied vibration, the mentioned noise sources and voltage fluctuations caused by the pyroelectric effect in the PZT and PVDF transducers. Shielded cables are used during measurements, but external noise sources can still be coupled into the system.

3.2.2 TEG Random Number Generation

The thermal noise, shot noise and generation-recombination noise sources discussed in Section 2.2.2 contributes to the noise signal output from the thermoelectric generator. The noise signal from the thermoelectric generator is generated by first applying a low ΔT across the thermoelectric generator as seen in Figure 3.5. Just like the output of the piezoelectric transducer, the measured output from the thermoelectric generator is also relatively weak and must be amplified with an external amplifier circuit. The amplified signal is then sampled/recorded with a data acquisition tool for further statistical analysis.

Figure 3.5: Block Diagram of TEG Random Number Generator.

The analyzed noise signal is a combination of the generated voltage output from the applied ΔT, the mentioned noise sources and voltage fluctuations caused by small temperature fluctuations during testing.

3.2.3 Solar Cell Random Number Generation

The output noise signal generated by the solar cell is attributed to various sources including the thermal noise, shot noise and generation-recombination noise discussed in Section 2.2.2. The noise signal from the solar cell is generated by shining a light source of low intensity onto the solar cell as shown in Figure 3.6. The produced electrical signal is then amplified and sampled/recorded with the data acquisition tool.

Figure 3.6: Block Diagram of Solar Cell Random Number Generator.

The analyzed noise signal is a combination of the mentioned noise sources and voltage fluctuations caused by temperature and light intensity fluctuations.

Chapter 4

Experiment Setups

This chapter describes the fashion in which the transducers were tested. Sections 4.1-4.3 describe the PUF and RNG experiment setups for each transducer.

4.1 Piezoelectric Test Configuration

Five lead zirconate titanate (PZT) piezoelectric samples from Mide Technology Corporation [32] and five polyvinylidene fluoride (PVDF) samples from Measurement Specialties [33] were used during the PUF tests. The same five PZT samples and five PVDF samples were used during the RNG tests.

4.1.1 Resonance Frequency PUF

As shown in Figure 4.1, the piezo is mounted and clamped in a cantilever position. This allows the piezo to oscillate freely when excited by the impedance analyzer. The impedance analyzer is connected to the piezo via the flat electrodes of the piezo. The impedance analyzer is used to measure the impedance response of the piezo and find the series and parallel resonance frequencies of the device.

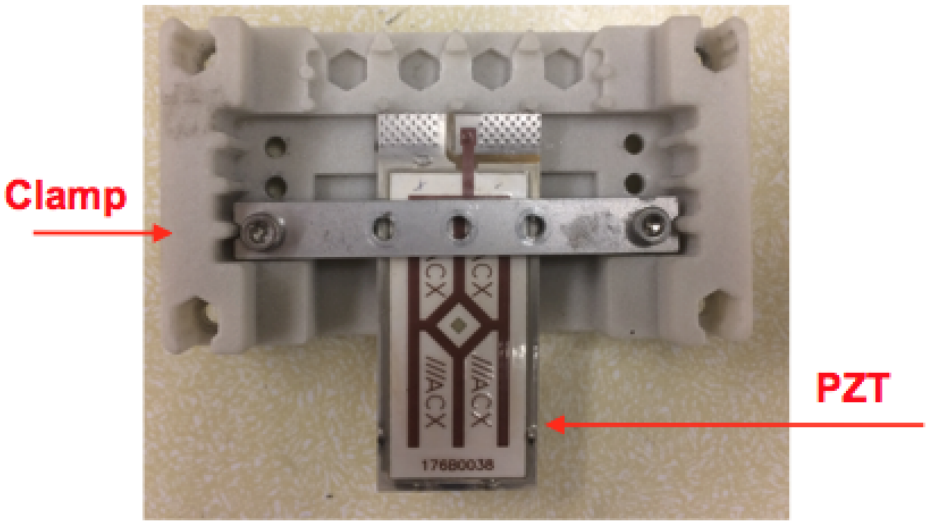

Figure 4.1: PUF Testing Setup of Piezoelectric Device.

In order to maintain consistent test runs, the experiment setup has to remain the same for each sample. The piezo is clamped and mounted in the recommended fixture and clamp location (Clamp '0') from Mide Tech [32]. This allows for every sample to be in the same starting location/position during testing. The screws on the clamp are checked with a torque wrench to ensure the same clamping force on each sample under test. No mass is attached to the unclamped end of the piezo samples. Each sample was tested more than once and a five minute wait time was issued between test runs to allow the system to settle before running the test again.

Initial test runs measured various aspects of the output signal, but after analysis of the preliminary data, the resonance frequency measurements proved to be a good candidate for a potential PUF. The samples were also placed in a heat chamber and the resonance frequencies were once again measured. The samples were tested under temperatures ranging from 25°C to 150°C.

4.1.2 Vibration to Random Number Generation

A similar test setup is shown in Figure 4.2 for RNG testing. The difference being, now there is a function generator driving a vibration shaker that will produce a vibration signal onto the piezo sample. The output electrical signal is then passed through an amplifying circuit and recorded with the data acquisition system.

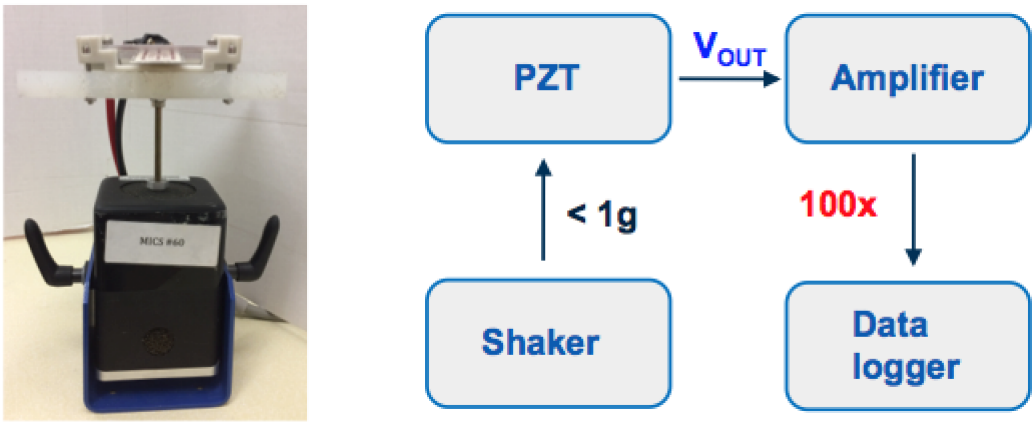

(a) Vibration Shaker.

(b) Piezo RNG Block Diagram.

Figure 4.2: RNG Testing Setup of Piezoelectric Device.

The piezo samples are in the same clamped position and location on the mounting fixture. The mount, along with the samples, are attached on top of the shaker. The function generator is set to its minimum frequency and amplitude settings of 1Hz and 10mV respectively. The shaker is monitored with an accelerometer to measure the amount of force being applied to the piezo samples. The output from the samples are fed through an amplifier circuit with a set gain of 100. The amplified signal is then measured on the ADC pin of the NI USB 6211 to convert the analog signal to binary data. 10 million bits worth of binary data is collected for each test sample. The binary data is later used to run the NIST Statistical Test Suite. The amplitude and frequency to drive the shaker is then increased and the same measurements are made for every new function generator until the output signal of the amplifier shows clipping.

4.2 Thermoelectric Generator Test Configuration

Five thermoelectric generator samples from TECTEG Company [34] were used during the PUF and RNG tests. The thermoelectric generator is placed between a hotplate and heatsink. A thermocouple monitors the temperatures on both sides of the thermoelectric generator and the data acquisition system collects the data. The only difference between the PUF and RNG test setup, is the addition of the amplifier circuit for the RNG test measurements.

4.2.1 Temperature Controlled OCV PUF

Figure 4.3, shows that the hotplate is the heating element used to apply heat onto the hot side of the thermoelectric generator. A heatsink is attached to the cool side of the TEG via

thermal grease. A 12V fan is mounted on top of the heatsink and powered by an external DC power supply. The thermocouple measures the temperature of the hot and cold side of the TEG. The output voltage data is then captured with the DAQ system.

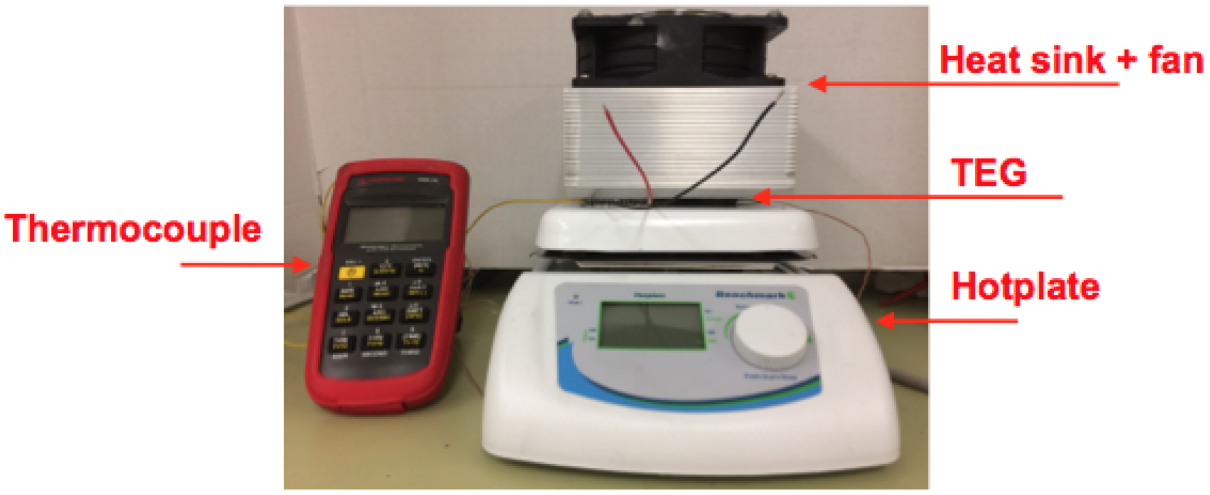

Figure 4.3: PUF/RNG Testing Setup of Thermoelectric Generator.

Each TEG sample is placed in the same location between the hotplate and heatsink. The hotplate and heatsink run for 1hr before any measurements are taken to allow for temperature steady state to take place. The temperature is verified with the thermocouple and the temperature feedback sensor on the hotplate. The tests are ran at a temperature difference of 5°C. The heatsink and fan maintain the temperature of the cool side on the TEG close to room temperature, and the hotplate is set to be 5°C hotter than the cool side. The open circuit voltage measurements are recorded for 30 minutes with the data acquisition system.

4.2.2 Thermal Gradient to Random Number Generation

Figure 4.4 displays a similar setup to Figure 4.3 with exception to the amplifier circuit used in the RNG testing.

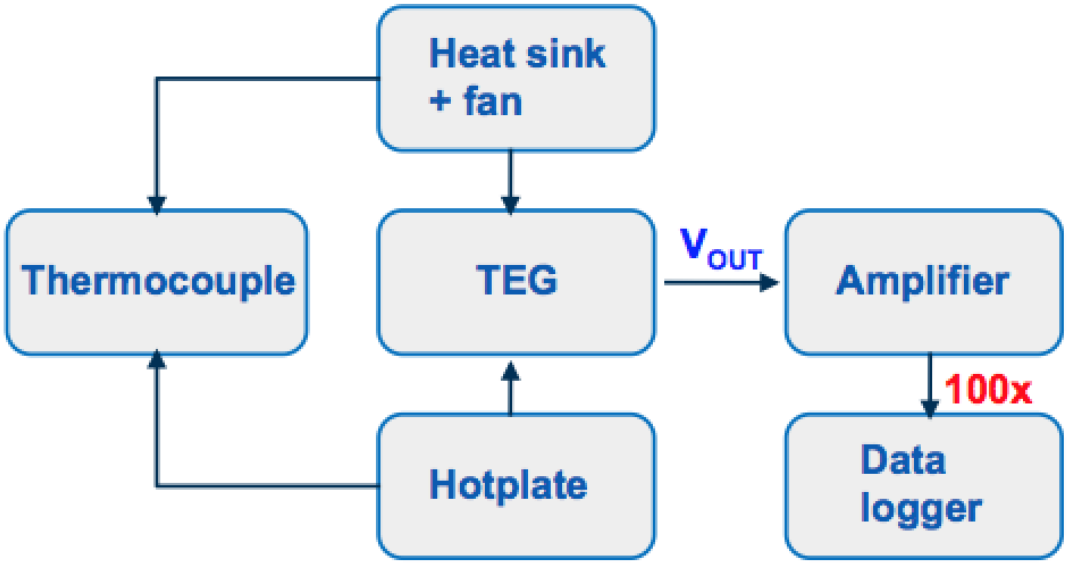

Figure 4.4: Block Diagram of RNG Testing Setup for Thermoelectric Generator.

The same test procedure from Section 3.3.1 is applied to the TEG samples for RNG testing. For the RNG tests, the temperature difference across the TEG samples is less than 1°C initially, and later increased to normal temperature ratings during other test runs. The electrical output signal is passed through the amplifier circuit with a gain of 100 and then read on the ADC pin of the data acquisition system to be converted into binary data and later used by the NIST Statistical Test Suite.

4.3 Solar Cell Test Configuration

Five 0.5W mono-crystalline silicon solar cell samples from Sunnytech [35] were used during the PUF tests. A solar cell and remote controlled light source mounted in an enclosure are utilized. A thermocouple monitors the temperature inside the test environment and the data acquisition system collects the data. The same five solar cell samples are used in the RNG testing. A light meter is used to measure the light exposure of the samples. A black film is used to cover the samples during testing.

4.3.1 Light Controlled OCV PUF

Figure 4.5, shows an RGB LED light bulb as the light source for the solar cells. The LED is connected directly to a wall outlet. The LED and solar cell samples are housed in an enclosure with a thermocouple measuring the inside temperature of the enclosure. A remote control

is used to cycle through the various color light sources on the LED. The data acquisition system records the open circuit voltage of the samples.

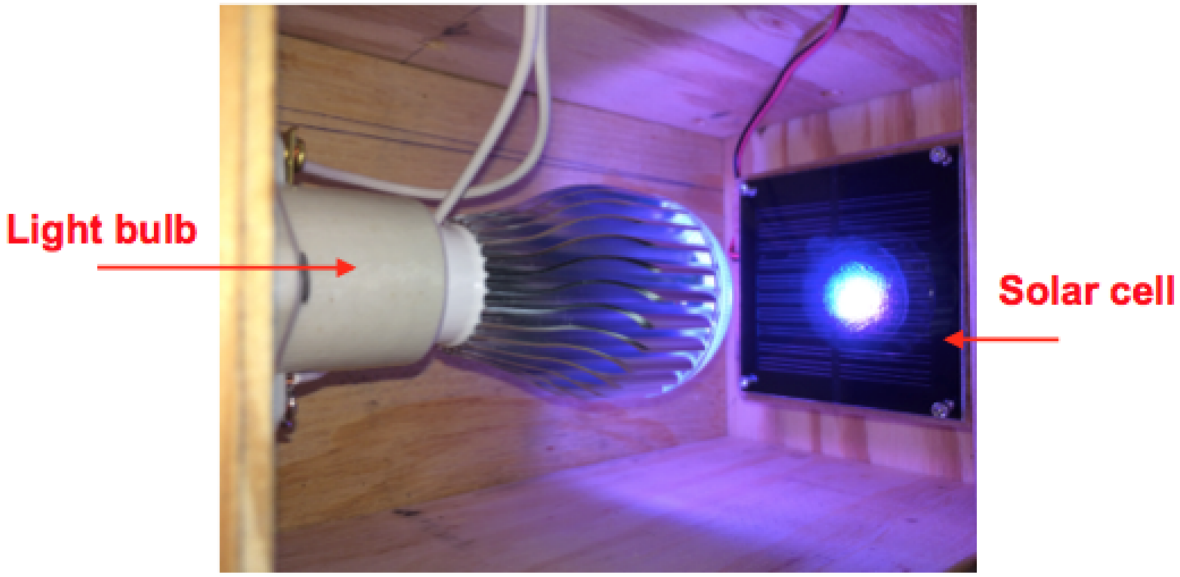

Figure 4.5: PUF Testing Setup of Solar Cell.

Each solar cell sample is placed in the same position and location inside the enclosure. Once placed, the light source is turned on and the inside temperature of the enclosure is measured for 30 minutes to allow for temperature steady state to occur within the enclosure. The experiment is then run by cycling through the RGB LED from white to red to blue to green, and measuring the open circuit voltage at each wavelength for 30 minutes with the DAQ system.

4.3.2 Ambient Light to Random Number Generation

In Figure 4.6, the block diagram shows an ambient light as the light source for the solar cells. The light is filtered through films of various transparencies and opaqueness. A thermocouple measures the temperature of the sample. The output electrical signal is passed through an amplifier and the amplified signal is measured with the data acquisition system.

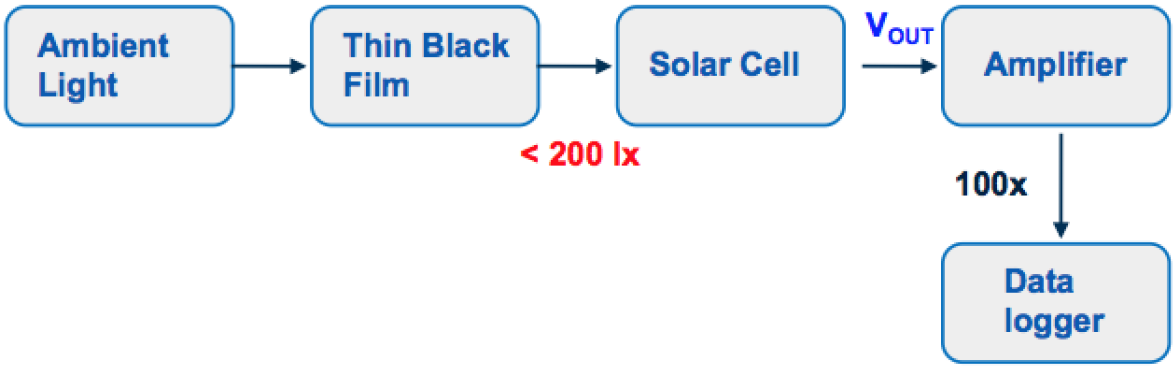

Figure 4.6: Block Diagram of RNG Testing Setup for Solar Cell.

The temperature of each sample is measured to ensure the same testing conditions during measurements. A light meter is used to measure the amount of light exposure the sample is under when applying the light-filtering film. The output signal from the solar cell is then amplified with a gain of 100 and the amplified signal is then measured with data acquisition system. The initial test begins with the light exposure set to less than 200lx and then varied until the light exposure reaches normal levels of light intensity.

Chapter 5

Measurement Results

This chapter describes the measurement results of each transducer for the PUF and random number generation. Sections 5.1-5.3 describe the PUF and RNG measurement results for each transducer. Lastly, the results from each transducer are compared in Section 5.4.

5.1 Piezoelectric Test Results

This section discusses the PUF and random number generation measurement results for the PZT piezoelectric transducers.

5.1.1 Resonance Frequency PUF Results

As seen in Tables 5.1 and 5.2, the series and parallel resonance frequencies among the different piezoelectric samples differs. The piezo samples were tested over a 10 day period where a 24-hr interval was implemented between each test. The average of the results over the 10 day period was calculated, as well as the standard deviation of the data samples.

Figure 5.1 shows the impedance response for the five piezo samples. The series resonance frequency is highlighted in the blue circles and the parallel resonance frequency is highlighted in the red circles.

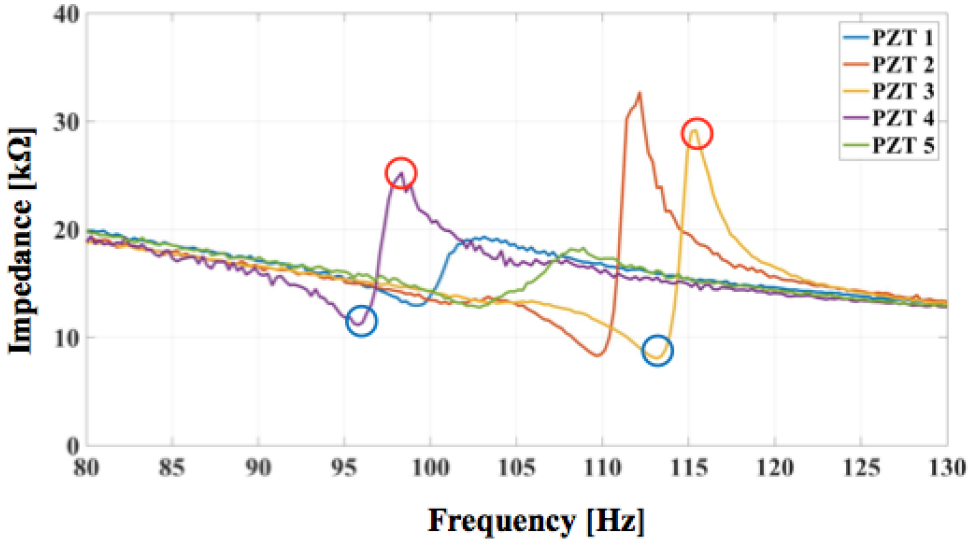

Figure 5.1: Piezo Impedance Response.

Over the 10-day testing period the series resonance frequencies remained relatively stable as the standard deviation was less than 0.1 Hz for each sample.

Table 5.1: Piezo Series Resonance Frequency Measurements

Period	Frequency [Hz]				
	1	2	3	4	5
Day 1	98.811	109.501	113.625	96.555	103.218
Day 2	98.923	109.652	113.764	96.576	103.397
Day 3	98.942	109.423	113.542	96.487	103.263
Day 4	98.761	109.544	113.622	96.599	103.239
Day 5	98.872	109.405	113.609	96.403	103.173
Day 6	98.991	109.598	113.71	96.534	103.247
Day 7	98.803	109.667	113.697	96.641	103.362
Day 8	98.713	109.545	113.734	96.578	103.249
Day 9	98.967	109.411	113.656	96.677	103.154
Day 10	98.944	109.531	113.671	96.561	103.288
Mean and Standard Deviation					
μ	98.8727	109.5277	113.663	96.5611	103.259
σ	0.095	0.094	0.066	0.076	0.075

Over the 10-day testing period the parallel resonance frequencies remained relatively stable as the standard deviation was less than 0.1 Hz for most samples.

Table 5.2: Piezo Parallel Resonance Frequency Measurements

Period	Frequency [Hz]				
	1	2	3	4	5
Day 1	103.444	112.612	115.234	97.755	108.498
Day 2	103.331	112.744	115.213	97.617	108.312
Day 3	103.446	112.677	115.061	97.71	108.409
Day 4	103.475	112.683	115.202	97.806	108.431
Day 5	103.207	112.826	115.292	97.792	108.244
Day 6	103.433	112.687	115.254	97.744	108.411
Day 7	103.32	112.538	115.116	97.531	108.403
Day 8	103.409	112.599	115.284	97.729	108.755
Day 9	103.489	112.606	115.273	97.689	108.476
Day 10	103.516	112.614	115.346	97.701	108.681
Mean and Standard Deviation					
μ	103.407	112.6586	115.2275	97.7074	108.462
σ	0.094	0.083	0.085	0.082	0.154

The same piezo transducers were then tested over a different 10 day period, in which they were subjected to an increase in temperature while under testing. As the piezoelectric transducers reached higher temperatures within the heating chamber, the measured resonance frequency values varied from the previously stated means in Table 5.1. This is due to the nature of the data logging device and the signal output at higher temperatures. Figure 5.2 shows a typical piezo transducer output waveform at relative room temperature and at higher temperatures. When the piezoelectric transducer is tested at higher temperatures, the output signal sees a reduction in the amplitude of the signal along with coupled noise. This gives rise to error when sampling the signal for measurements.

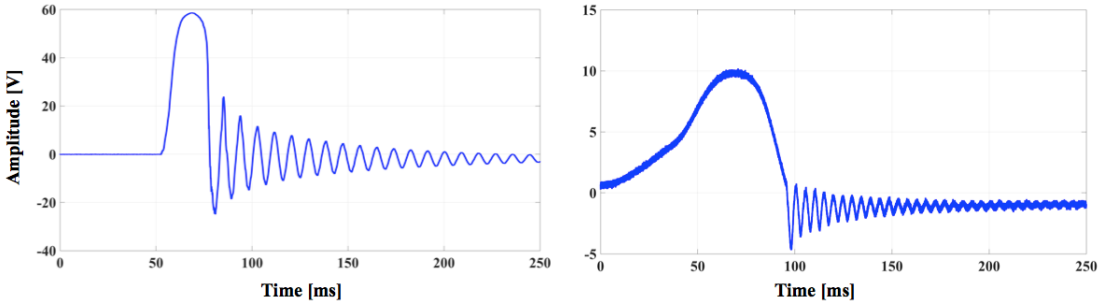

(a) $\Delta T = 27°C$ (b) $\Delta T = 150°C$

Figure 5.2: Amplitude Reduction at Higher Temperatures.

5.1.2 Vibration to Random Number Generation Results

Figure 5.3 shows the random output voltage signal from one piezoelectric transducer when excited with a low g-force input and passed through an amplifier with a gain setting of 100.

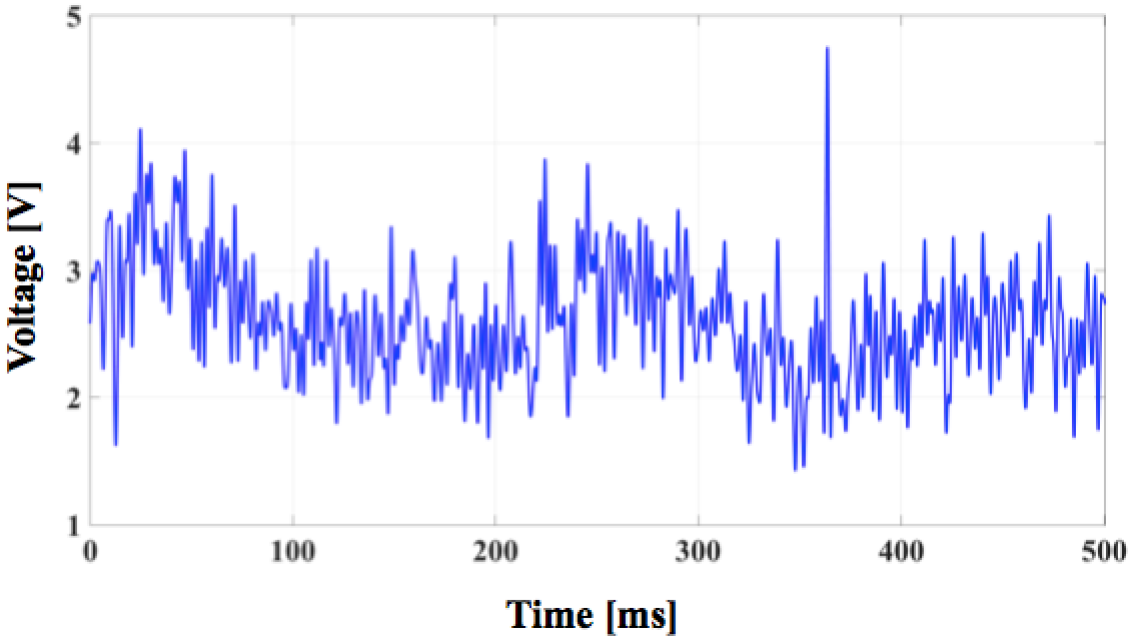

Figure 5.3: Noise Signal Output from Piezoelectric Device.

The noise signal is collected via the data logger and then processed in Matlab to analyze its distribution. Figure 5.4 shows the probability density function (PDF) of the data with the blue curve representing the measured data, and the red curve representing a Gaussian distribution. As can be seen in the figure, the data collected from the noisy signal resembles a Gaussian distribution, but further tests are carried out to ensure the data appears random.

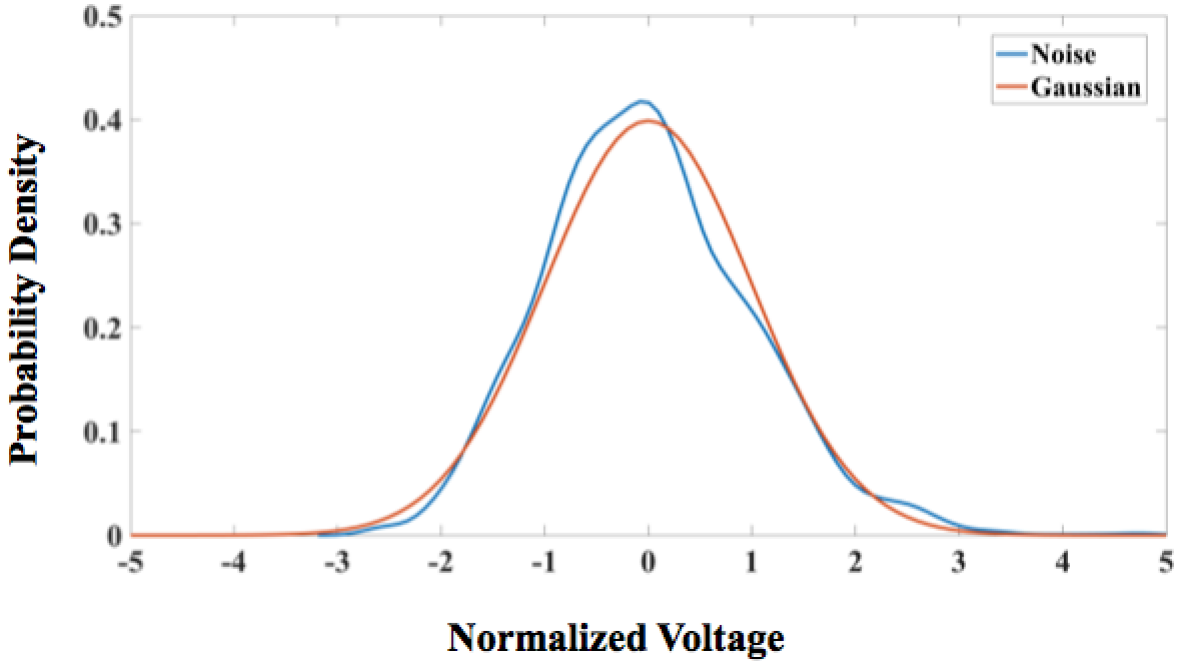

Figure 5.4: Piezo Noise Signal Distribution (blue), Gaussian Distribution (red).

One piezo transducer generated 10 million bits worth of data, with 1 million bits worth of data considered as one sequence used for one run of tests. Table 5.3 highlights the results from the NIST Statistical Analysis for 10 test runs on one piezo sample.

Table 5.3: Piezo RNG NIST Statistical Analysis

Random Number Generation Test	# of Passed Sequences
Frequency (Monobit)	9/10
Frequency Test within a Block	10/10
Runs	9/10
Longest-Run-of-Ones in a Block	9/10
Binary Matrix Rank	9/10
Discrete Fourier Transform (Spectral)	10/10
Non-overlapping Template Matching	8/10
Overlapping Template Matching	9/10
Maurer's "Universal Statistical"	9/10
Linear Complexity	8/10
Serial	10/10
Approximate Entropy	9/10
Cumulative Sums (Cusums)	9/10
Random Excursions	8/8
Random Excursions Variant	7/8

The results show that the generated data from the transducer passed the NIST Statistical Test Suite battery of tests. The minimum pass rate for each statistical test with the exception of the random excursion (variant) test is approximately = 8 for a sample size = 10 binary sequences. The minimum pass rate for the random excursion (variant) test is approximately = 7 for a sample size = 8 binary sequences. This means that for any given test, if more than 7 or 8 sequences passed respectively, then the generated data passed the data. The 10 sequences represent 1,000,000 bits of data for each sequence.

The plots shown in Figure 5.5 are probability density functions of the piezoelectric sensor at different vibration excitation levels. The lower vibration excitation generates a probability density function that closer resembles a Gaussian distribution. The higher vibration excitation at a normal operating level, produces a probability density function that is nowhere near resembling a Gaussian distribution.

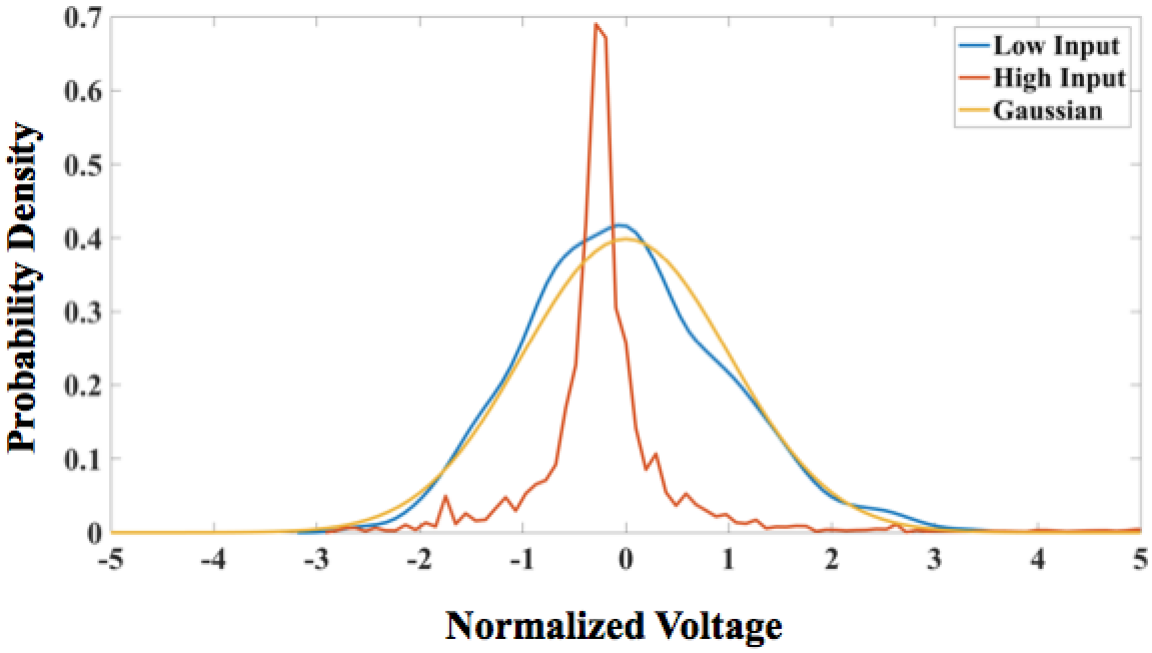

Figure 5.5: Piezo Noise Signal Distribution for Different Excitation Amplitudes.

5.2 Thermoelectric Generator Test Results

This section discusses the PUF and random number generation measurement results for the thermoelectric generators.

5.2.1 Temperature Controlled OCV PUF Results

As seen in Figure 5.6, the open-circuit voltages of the five thermoelectric generators were measured over a 30-minute period at a ΔT of 5°C, allowing enough time for voltage steady-state to occur. The measured voltages fluctuated over time due to the temperature variations of the hotplate and heat sink.

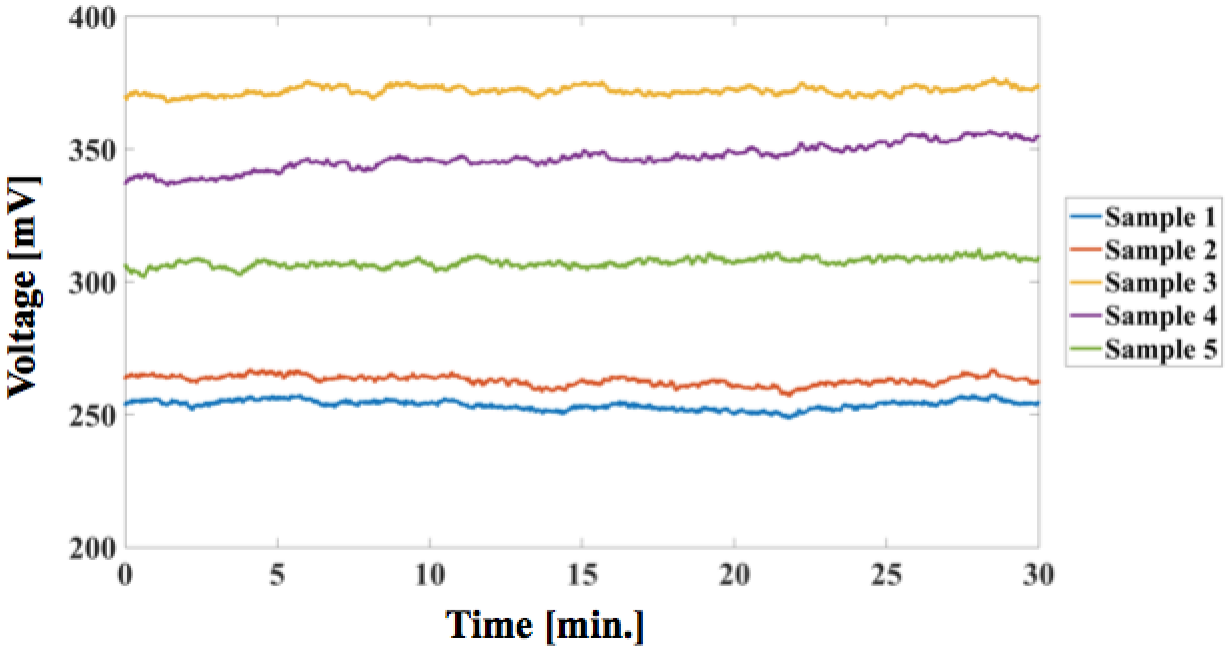

Figure 5.6: Open Circuit Voltage of Thermoelectric Generators at $\Delta T = 5°C$.

The temperature was monitored throughout the experiment, but small temperature variations unmeasurable by the thermocouple can cause significant voltage swings on the output. Therefore the average of the voltage readings over time were taken as the open-circuit voltage for each thermoelectric generator. Table 5.4, shows the open-circuit voltage measurements over a 10-day period at the same ΔT of 5°C. The mean and standard deviation were also calculated to highlight the variation in the open-circuit voltage measurements for each thermoelectric generator.

Table 5.4: TEG Open-Circuit Voltage

Period	Voltage [mV]				
	1	2	3	4	5
Day 1	253.7	262.9	372.1	346.9	307.4
Day 2	255.1	264.2	371.1	343.5	304.2
Day 3	248.3	260.4	373.9	347.1	310.3
Day 4	250.7	262.1	372.5	343.3	305.5
Day 5	248.9	263.5	372.2	349.1	307.6
Day 6	256.2	265.1	374.5	350.4	304.5
Day 7	254.8	265.6	373.5	343.9	308.4
Day 8	251.1	259.7	371.2	347.4	305.1
Day 9	257.5	260.6	372.4	346.6	309.2
Day 10	255.4	261.7	374.1	342.9	309.8
Mean and Standard Deviation					
μ	253.17	262.58	372.75	346.11	307.2
σ	3.195	2.028	1.192	2.598	2.2509

The measurement results show variations in the open-circuit voltage over the ten day testing period. This can be contributed to the heatsink and hotplate not maintaining a constant temperature over time. The mean voltage readings for each thermoelectric generator differ between each sample. Another contributing factor may be the amount of applied thermal grease, which can increase or decrease the thermal conductivity between the thermoelectric generator and hotplate or heatsink.

5.2.2 Thermal Gradient to Random Number Generation Results

Figure 5.7 shows the random output voltage signal from one thermoelectric generator transducer when excited with a low ΔT input and passed through an amplifier with a gain setting of 100.

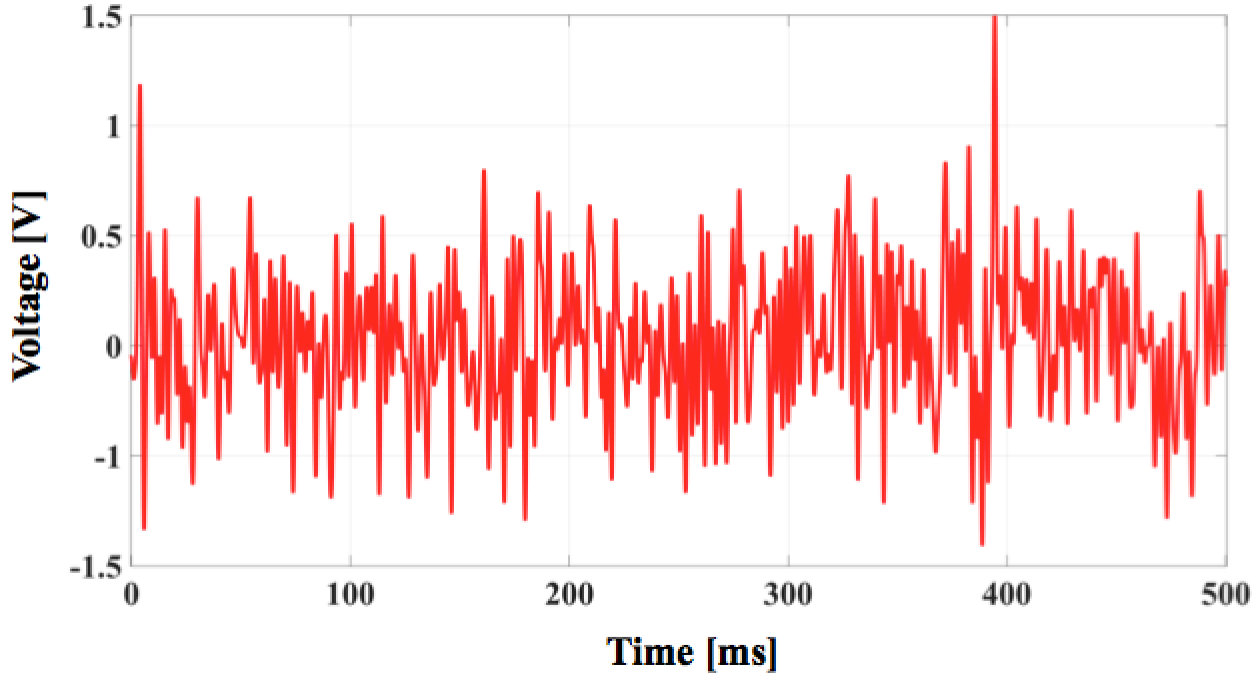

Figure 5.7: Noise Signal Output from Thermoelectric Generator.

The noise signal is collected via the data logger and then processed in Matlab to analyze its distribution. Figure 5.8 shows the probability density function (PDF) of the data with the blue curve representing the measured data, and the red curve representing a Gaussian distribution. As can be seen in the figure, the data collected from the noisy signal resembles a Gaussian distribution, but further tests are carried out to ensure the data appears random.

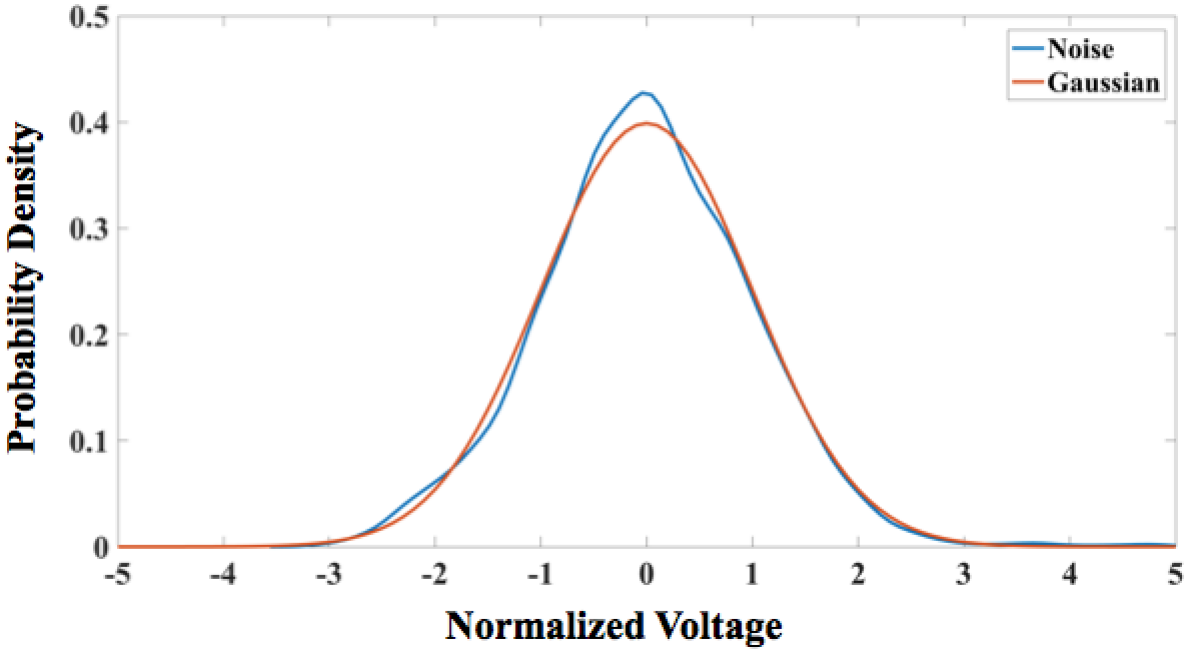

Figure 5.8: TEG Noise Signal Distribution (blue), Gaussian Distribution (red).

One thermoelectric generator transducer generated 10 million bits worth of data, with 1 million bits worth of data considered as one sequence used for one run of tests. Table 5.5 highlights the results from the NIST Statistical Analysis for 10 test runs on one TEG sample.

Table 5.5: TEG RNG NIST Statistical Analysis

Random Number Generation Test	# of Passed Sequences
Frequency (Monobit)	10/10
Frequency Test within a Block	10/10
Runs	9/10
Longest-Run-of-Ones in a Block	9/10
Binary Matrix Rank	9/10
Discrete Fourier Transform (Spectral)	10/10
Non-overlapping Template Matching	9/10
Overlapping Template Matching	9/10
Maurer's "Universal Statistical"	9/10
Linear Complexity	9/10
Serial	10/10
Approximate Entropy	10/10
Cumulative Sums (Cusums)	9/10
Random Excursions	8/8
Random Excursions Variant	8/8

The results show that the generated data from the transducer passed the NIST Statistical Test Suite battery of tests. The minimum pass rate for each statistical test with the exception of the random excursion (variant) test is approximately = 8 for a sample size = 10 binary sequences. The minimum pass rate for the random excursion (variant) test is approximately = 7 for a sample size = 8 binary sequences. This means that for any given test, if more than 7 or 8 sequences passed respectively, then the generated data passed the data. The 10 sequences represent 1,000,000 bits of data for each sequence.

The plots shown in Figure 5.9 are probability density functions of the thermoelectric generator transducers at different thermal excitation levels. The lower thermal excitation generates a probability density function that closer resembles a Gaussian distribution. The higher thermal excitation at a normal operating level, produces a probability density function that strays away from the ideal Gaussian distribution.

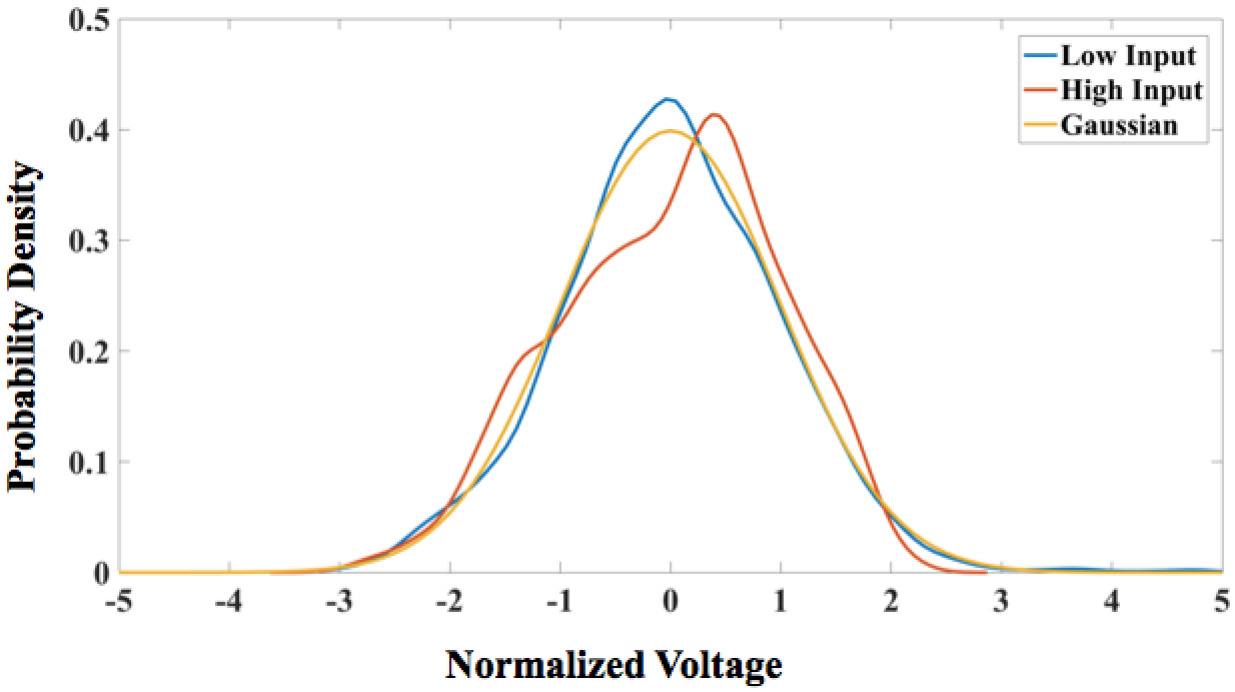

Figure 5.9: TEG Noise Signal Distribution for Different Excitation Amplitudes.

5.3 Solar Cell Test Results

This section discusses the PUF and random number generation measurement results for the solar cells.

5.3.1 Light Controlled OCV PUF Results

As seen in Figure 5.10, the open-circuit voltages of the five solar cells were measured over a 30-minute period at a light intensity of 2,000lx, allowing enough time for voltage steady-state to occur. The measured voltages fluctuated over time due to the temperature variations generated by the light bulb and surrounding environment.

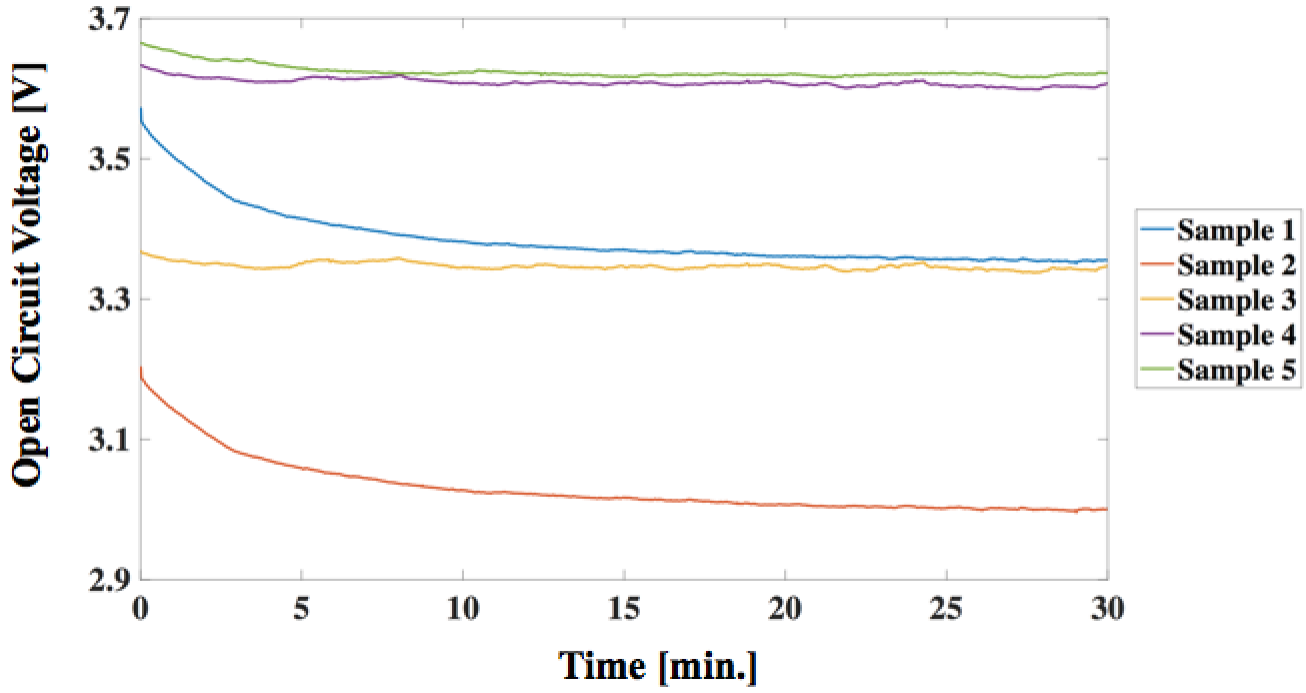

Figure 5.10: Open Circuit Voltage of Solar Cells at 2,000lx.

The heat generated by the light source and the change in temperature of the surrounding environment can cause changes in the voltage readings from the solar cell. Therefore the average of the voltage readings over time were taken as the open-circuit voltage for each solar cell. Table 5.6, shows the open-circuit voltage measurements over a 10-day period at the same light intensity of 2,000lx. The mean and standard deviation were also calculated to highlight the variation in the open-circuit voltage measurements for each solar cell.

Table 5.6: Solar Cell Open-Circuit Voltage at 2,000lx

Period	Voltage [V]				
	1	2	3	4	5
Day 1	3.354	3.010	3.341	3.601	3.619
Day 2	3.353	3.007	3.344	3.600	3.617
Day 3	3.349	3.012	3.339	3.598	3.620
Day 4	3.351	3.007	3.342	3.602	3.635
Day 5	3.358	3.011	3.334	3.601	3.610
Day 6	3.350	3.012	3.341	3.600	3.615
Day 7	3.357	3.008	3.337	3.599	3.611
Day 8	3.354	3.011	3.336	3.604	3.632
Day 9	3.349	3.009	3.345	3.602	3.630
Day 10	3.359	3.010	3.340	3.591	3.624
Mean and Standard Deviation					
μ	3.353	3.009	3.339	3.599	3.621
σ	0.0037	0.0019	0.0035	0.0035	0.0087

The measurement results show variations in the open-circuit voltage over the ten day testing period. This can be contributed to small varying temperatures over time. The mean voltage readings for each solar cell differ between each sample. Another contributing factor may be any debris that may have stuck onto the solar cell in between tests that can cause a reduction in voltage readings by blocking out the light source.

5.3.2 Ambient Light to Random Number Generation Results

Figure 5.11 shows the random output voltage signal from one solar cell transducer when excited with a light intensity of less than 200lx input and passed through an amplifier with a gain setting of 100.

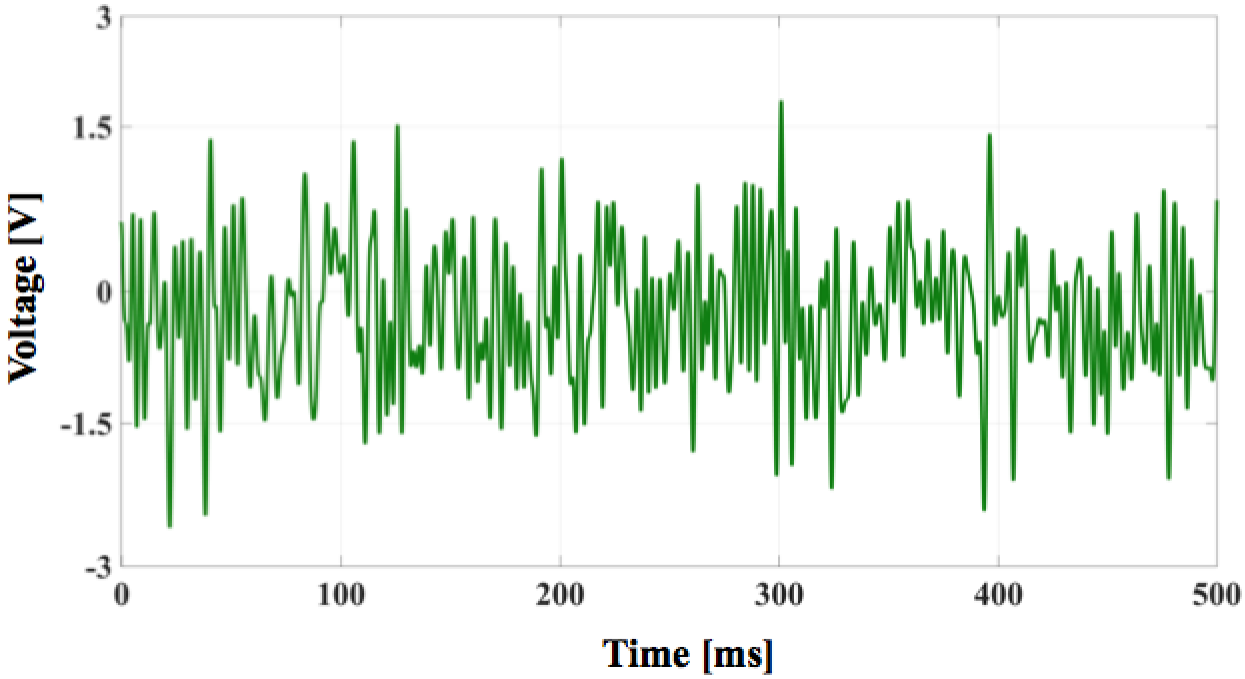

Figure 5.11: Noise Signal Output from the Solar Cell.

The noise signal is collected via the data logger and then processed in Matlab to analyze its distribution. Figure 5.12 shows the probability density function (PDF) of the data with the blue curve representing the measured data, and the red curve representing a Gaussian distribution. As can be seen in the figure, the data collected from the noisy signal resembles a Gaussian distribution, but further tests are carried out to ensure the data appears random.

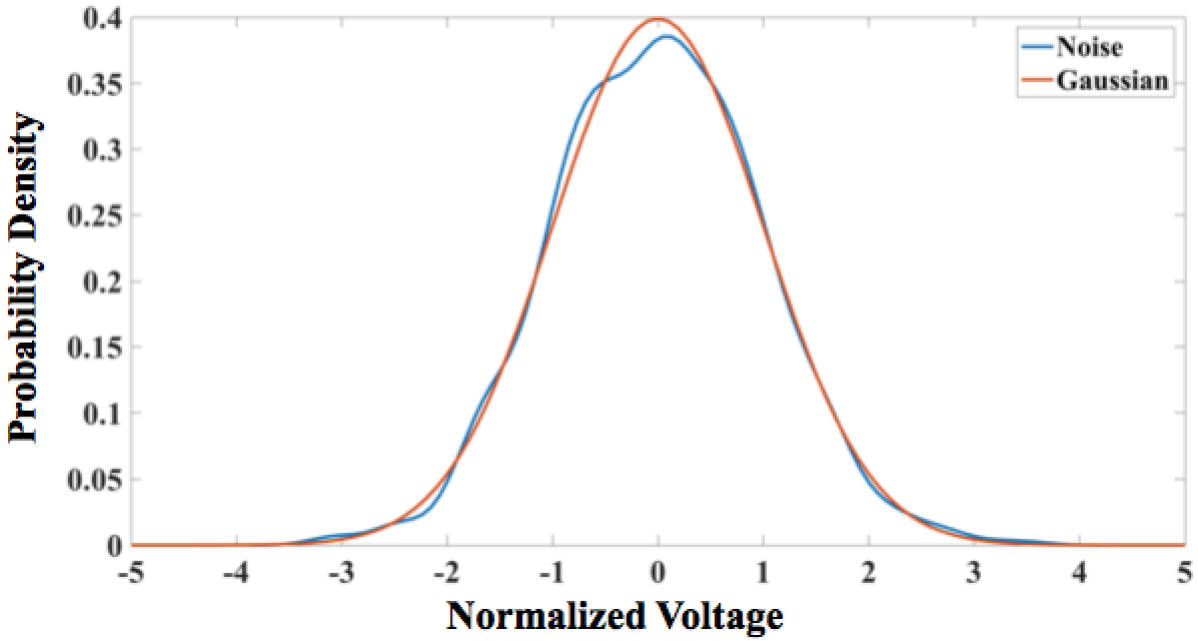

Figure 5.12: Solar Cell Noise Signal Distribution (blue), Gaussian Distribution (red).

One solar cell transducer generated 10 million bits worth of data, with 1 million bits worth of data considered as one sequence used for one run of tests. Table 5.7 highlights the results from the NIST Statistical Analysis for 10 test runs on one solar cell sample.

Table 5.7: Solar Cell RNG NIST Statistical Analysis

Random Number Generation Test	# of Passed Sequences
Frequency (Monobit)	9/10
Frequency Test within a Block	10/10
Runs	8/10
Longest-Run-of-Ones in a Block	9/10
Binary Matrix Rank	9/10
Discrete Fourier Transform (Spectral)	10/10
Non-overlapping Template Matching	9/10
Overlapping Template Matching	9/10
Maurer's "Universal Statistical"	9/10
Linear Complexity	9/10
Serial	10/10
Approximate Entropy	9/10
Cumulative Sums (Cusums)	9/10
Random Excursions	7/8
Random Excursions Variant	8/8

The results show that the generated data from the transducer passed the NIST Statistical Test Suite battery of tests. The minimum pass rate for each statistical test with the exception of the random excursion (variant) test is approximately = 8 for a sample size = 10 binary sequences. The minimum pass rate for the random excursion (variant) test is approximately = 7 for a sample size = 8 binary sequences. This means that for any given test, if more than 7 or 8 sequences passed respectively, then the generated data passed the data. The 10 sequences represent 1,000,000 bits of data for each sequence.

The plots shown in Figure 5.13 are probability density functions of the solar cell transducers at different light intensity excitation levels. The lower light intensity excitation generates a probability density function that closer resembles a Gaussian distribution. The higher light intensity excitation at a normal operating level, produces a probability density function that strays away from the ideal Gaussian distribution.

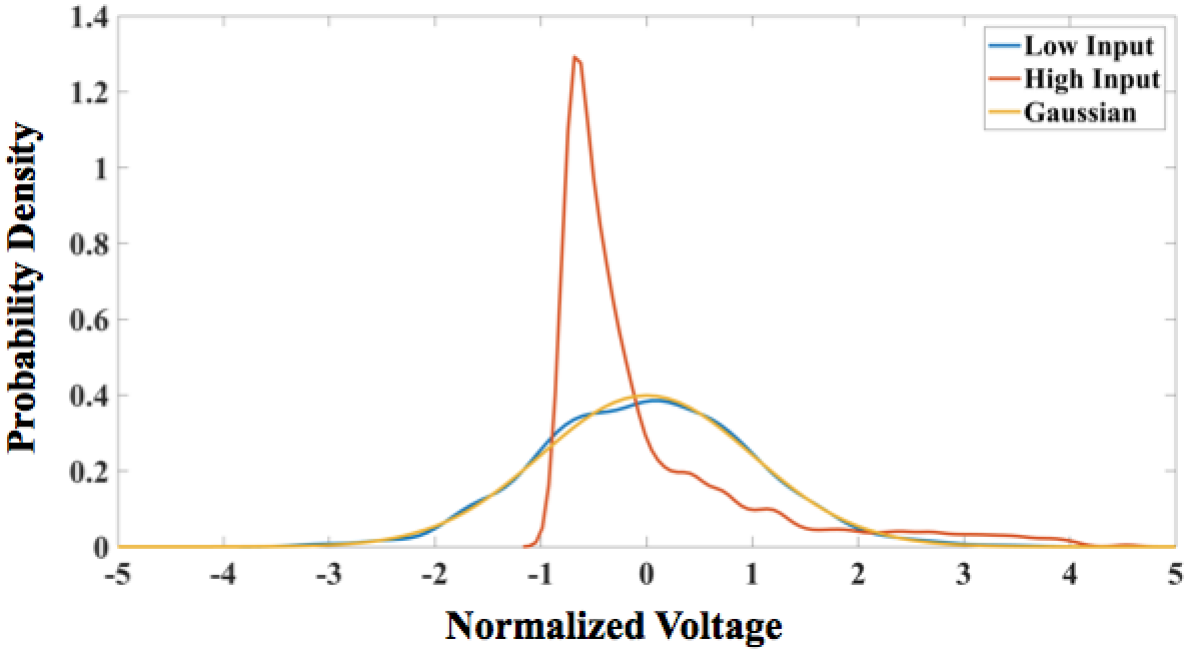

Figure 5.13: Solar Noise Signal Distribution for Different Excitation Amplitudes.

5.4 Comparisons

This section compares the PUF and random number generation results among the three different transducers.

Table 5.8 highlights the calculated results from the measured data for the thermoelectric generator OCV PUF, solar cell OCV PUF and piezo resonance frequency PUF. The coefficient of variation is calculated to evaluate how much the data varied across the five samples for each transducer. The PVDF results were omitted from this table since this evaluation is based on the spread of standard deviations and the PVDF results were very similar to the PZT results for this evaluation parameter.

Table 5.8: PUF Summary of Results

TEG	1	2	3	4	5	Coefficient of Variation
μ [mV]	253.17	262.58	372.75	346.11	307.2	0.76%
σ [mV]	3.195	2.028	1.192	2.598	2.251	
Solar Cell	1	2	3	4	5	Coefficient of Variation
μ [V]	3.353	3.009	3.339	3.599	3.621	0.61%
σ [V]	0.0037	0.0019	0.0035	0.0035	0.0087	
PZT	1	2	3	4	5	Coefficient of Variation
μ_{series} [Hz]	98.8727	109.5277	113.663	96.5611	103.259	**0.08%**
σ_{series} [Hz]	0.095	0.094	0.066	0.076	0.075	
μ_{parallel} [Hz]	103.407	112.6586	115.2275	97.7074	108.462	**0.09%**
σ_{parallel} [Hz]	0.094	0.083	0.085	0.082	0.154	

Based on the calculated results, the resonance frequency PUF from the piezoelectric transducer is a viable approach for PUF generation and implementation. The piezo PUF shows the lowest coefficient of variation which correlates to a high reproducibility rate of responses. The thermoelectric generator and solar cell can also be used as PUFs, but would require a form of signal processing to compensate for errors.

Table 5.9 highlights the results from the battery of tests in the NIST Statistical Test Suite for each transducer.

Table 5.9: Random Number Generation Summary of Results

Random Number Generation Test	# of Passed Sequences		
	Piezo	TEG	Solar Cell
Frequency (Monobit)	9/10	10/10	9/10
Frequency Test within a Block	10/10	10/10	10/10
Runs	9/10	9/10	8/10
Longest-Run-of-Ones in a Block	9/10	9/10	9/10
Binary Matrix Rank	9/10	9/10	9/10
Discrete Fourier Transform (Spectral)	10/10	10/10	10/10
Non-overlapping Template Matching	8/10	9/10	9/10
Overlapping Template Matching	9/10	9/10	9/10
Maurer's "Universal Statistical"	9/10	9/10	9/10
Linear Complexity	8/10	9/10	9/10
Serial	10/10	10/10	10/10
Approximate Entropy	9/10	10/10	9/10
Cumulative Sums (Cusums)	9/10	9/10	9/10
Random Excursions	8/8	8/8	7/8
Random Excursions Variant	7/8	8/8	8/8

The # of passed sequences were observed in each transducer. Based on the NIST test output each transducer generated data that passed all of the tests. These three transducers are all capable of being used for random number generation, but the TEG seems more suitable based on the test results. The TEG only failed 8 sequences compared to the 13 and 12 sequences for the piezo and solar cell respectively.

Chapter 6

Conclusion

Transducers typically used in energy harvesting applications can potentially be used in security applications by producing physical unclonable functions and random number generation. This thesis research analyzes transducers and their intrinsic properties to extend their purpose beyond energy harvesting.

6.1 Key Contributions

This study on energy harvesting transducers provides a preliminary baseline to further investigate their implementation in cryptographic security applications by utilizing the transducers for PUF and random number generation. It exploits the physical manufacturing variations in the transducer samples to generate sample-specific electrical responses that are utilized in PUF generation. Those electrical responses include, the resonance frequencies from the piezoelectric transducer and the average open-circuit voltages from the thermoelectric generators and solar cells. These PUFs are categorized as weak PUFs due to their limited challenge-response pairs. This study also analyzes the transducers for random number generation purposes by applying a low input excitation to the transducers, and measuring the amplified output noise signal.

6.2 Future Improvements

The measurement results proved to be promising but, there are several ways to continue and improve this research. The first improvement being on the experiments and their setups. The improvement here would be to increase the sample size of the transducers to over 200 samples and run the same experiments on each one. From a statistical perspective, the larger the sample size, the surer one can be about the measured results and can draw clearer

conclusions on those results. Due to budget constraints, the samples for each transducer were limited as a typical lower-end market PZT transducer costs around $25, a thermoelectric generator costs about $30 and solar cell costs around $10. As far as the experiment setups go, by adding a water cooling system for the thermoelectric generator and solar cell tests, it can improve the output voltage measurements. A water cooling system will allow for the TEG cold side to remain at an absolute temperature and won't be as dependent on the surrounding environmental temperature. By keeping the solar cell cool, the effect from the generated heat in the light source can be reduced.

Furthermore the random number generation will require further analysis to prove that the generated data was a direct result from the transducer itself and not external noise sources. A stochastic model of the potential noise sources in each transducer can provide a method to map those sources to the generated data output.

Bibliography

[1] K. K. Khedo, R. Perseedoss, A. Mungur *et al.*, "A wireless sensor network air pollution monitoring system," *arXiv preprint arXiv:1005.1737*, 2010.

[2] O. Vermesan and P. Friess, *Building the hyperconnected society: IoT research and innovation value chains, ecosystems and markets*. River Publishers, 2015.

[3] S. Singh and H. K. Verma, "Security for wireless sensor network," *International Journal on Computer Science and Engineering*, vol. 3, no. 6, pp. 2393–2399, 2011.

[4] J. Sen, "Security in wireless sensor networks," *Wireless Sensor Networks: Current Status and Future Trends*, vol. 407, 2012.

[5] H. Alwan and A. Agarwal, "A secure mechanism for qos routing in wireless sensor networks," in *Electrical & Computer Engineering (CCECE), 2012 25th IEEE Canadian Conference on*. IEEE, 2012, pp. 1–4.

[6] S. Tarannum *et al.*, "Energy conservation challenges in wireless sensor networks: A comprehensive study," *Wireless Sensor Network*, vol. 2, no. 06, p. 483, 2010.

[7] B. Tong, Z. Li, G. Wang, and W. Zhang, "How wireless power charging technology affects sensor network deployment and routing," in *Distributed Computing Systems (ICDCS), 2010 IEEE 30th International Conference on*. IEEE, 2010, pp. 438–447.

[8] N. A. Bhatti, M. H. Alizai, A. A. Syed, and L. Mottola, "Energy harvesting and wireless transfer in sensor network applications: Concepts and experiences," *ACM Transactions on Sensor Networks (TOSN)*, vol. 12, no. 3, p. 24, 2016.

[9] K. Seema and S. Jebaraj, "Secure data collection in clustered wsns using digital signature," in *Current Trends in Engineering and Technology (ICCTET), 2014 2nd International Conference on*. IEEE, 2014, pp. 543–546.

[10] M. Al Ameen, J. Liu, and K. Kwak, "Security and privacy issues in wireless sensor networks for healthcare applications," *Journal of medical systems*, vol. 36, no. 1, pp. 93–101, 2012.

[11] D. Boneh, N. Modadugu, and M. Kim, "Generating rsa keys on a handheld using an untrusted server," in *International Conference on Cryptology in India*. Springer, 2000, pp. 271–282.

[12] E. Coca and V. Popa, *Third Generation Active RFID from the Locating Applications Perspective*. INTECH Open Access Publisher, 2011.

[13] B. Halak, M. Zwolinski, and M. S. Mispan, "Overview of puf-based hardware security solutions for the internet of things," in *Proc. IEEE 59th Int. Midwest Symp. Circuits and Systems (MWSCAS)*, Oct. 2016, pp. 1–4.

[14] S. Deyati, B. J. Muldrey, A. D. Singh, and A. Chatterjee, "Challenge engineering and design of analog push pull amplifier based physically unclonable function for hardware security," in *Proc. IEEE 24th Asian Test Symp. (ATS)*, Nov. 2015, pp. 127–132.

[15] R. Maes and I. Verbauwhede, "Physically unclonable functions: A study on the state of the art and future research directions," *Towards Hardware-Intrinsic Security*, Jan. 2010. [Online]. Available: http://dx.doi.org/10.1007/978-3-642-14452-3_1

[16] M. Stipevi and . K. Ko, "True random number generators," *Open Problems in Mathematics and Computational Science*, Jan. 2014. [Online]. Available: http://dx.doi.org/10.1007/978-3-319-10683-0_12

[17] "The bitbabbler black trng," Online. [Online]. Available: http://www.bitbabbler.org/what.html#BitBabbler-Black

[18] "Open hardware random number generator," Online. [Online]. Available: http://onerng.info

[19] "Purequantum model pq4000ks," Online. [Online]. Available: https://comscire.com/product/pq4000ks/

[20] U. Rhrmair and D. E. Holcomb, "Pufs at a glance," in *Proc. Automation Test in Europe Conf 2014 Design Exhibition (DATE)*, Mar. 2014, pp. 1–6.

[21] C. Herder, M. D. Yu, F. Koushanfar, and S. Devadas, "Physical unclonable functions and applications: A tutorial," *Proceedings of the IEEE*, vol. 102, no. 8, pp. 1126–1141, Aug. 2014.

[22] P. Sedlak, J. Majzner, and J. ikula, "Noise in piezoelectric ceramics at the low temperatures," *Radioengineering*, vol. 20, pp. 200–203, 2011.

[23] PI, "Piezo transducers in adaptronics for industry and automation," Online, 2012. [Online]. Available: http://www.piezo.ws/piezo_products/Piezo-Patch-Transducer/index.php

[24] A. Konczakowska and B. M. Wilamowski, *Fundamentals of Industrial Electronics*, J. D. Irwin, Ed., 2011.

[25] X. P. Zou, L. Y. Zhang, X. Yao, L. K. Wang, and F. X. Zhang, "Dielectric and pyroelectric properties of pzt-pvdf pyroelectric composites," *Ferroelectrics*, vol. 196, no. 1, pp. 105–108, 1997. [Online]. Available: http://dx.doi.org/10.1080/00150199708224143

[26] J. Richard, "How to build a homemade thermoelectric generator," 2017. [Online]. Available: http://topmagneticgenerator.com/build-homemade-thermoelectric-generator/

[27] 2017. [Online]. Available: http://www.hk-phy.org/energy/alternate/print/solar_phy_print_e.html

[28] R. Mller, "Generation-recombination noise," in *Noise in Physical Systems*. Springer, Jan. 1978. [Online]. Available: http://dx.doi.org/10.1007/978-3-642-87640-0_2

[29] A. Rukhin, J. Soto, J. Nechvatal, M. Smid, and E. Barker, "A statistical test suite for random and pseudorandom number generators for cryptographic applications," DTIC Document, Tech. Rep., 2001.

[30] Y. K. Ramadass and A. P. Chandrakasan, "A battery-less thermoelectric energy harvesting interface circuit with 35 mV startup voltage," *IEEE Journal of Solid-State Circuits*, vol. 46, no. 1, pp. 333–341, Jan. 2011.

[31] R. A. Sinton, A. Cuevas, and M. Stuckings, "Quasi-steady-state photoconductance, a new method for solar cell material and device characterization," in *Proc. Conf. Record of the Twenty Fifth IEEE Photovoltaic Specialists Conf. - 1996*, May 1996, pp. 457–460.

[32] M. Technology, "Ppa products datasheet and manual," Online. [Online]. Available: http://info.mide.com/piezo-products/download-piezo-products-datasheets

[33] M. S. Inc., "Piezo film sensors technical manual," Online. [Online]. Available: https://www.sparkfun.com/datasheets/Sensors/Flex/MSI-techman.pdf

[34] TECTEG, "Instructions and specifications," Online. [Online]. Available: http://tecteg.com/wp-content/uploads/2015/11/SPEC-SHEET-TEG2-126LDT.pdf

[35] Sunnytech, "Sunnytech 0.5w 5v 100ma mini solar panel," Online. [Online]. Available: http://www.solarproductswarehouse.com/inventory/2225799/